NATIONAL ADVISORY COMMITTEE FOR AERONAUTICS

TECHNICAL NOTE 2808

SHORT-BEARING APPROXIMATION FOR FULL JOURNAL BEARINGS

By F. W. Ocvirk

Cornell University

Washington

October 1952

NATIONAL ADVISORY COMMITTEE FOR AERONAUTICS

TECHNICAL NOTE 2808

SHORT-BEARING APPROXIMATION FOR FULL JOURNAL BEARINGS

By F. W. Ocvirk

SUMMARY

The mathematical analysis presented here is the result of attempts to compare existing solutions with the experimental data on pressure distribution in the oil film of a short journal bearing available in NACA TN 2507. It is apparent that the end leakage of oil flow has a predominant effect in narrow bearings, and that a simple approximation including end-leakage effects would be useful.

A mathematical function giving circumferential and axial pressure distribution in terms of eccentricity ratio or attitude was determined analytically. The solution includes endwise flow and that part of the circumferential flow which is proportional to journal surface velocity and varying film thickness but neglects the effect of pressure on the circumferential flow. The solution is fundamentally based on the Reynolds' equation but, like other solutions, neglects one term in order to make the integration possible. This solution neglects the term which has the least effect in narrow bearings, a method originally proposed by Michell and Cardullo.

The pressure-distribution function was extended to determine expressions giving applied load, attitude angle, location and magnitude of peak film pressure, friction, and required oil flow rate as functions of the eccentricity ratio. A basic nondimensional quantity resulting from this analysis is called the capacity number, which is the product of the Sommerfeld number and the square of the length-diameter ratio. With length-diameter ratio incorporated in the capacity number, bearing performance curves having capacity number as the abscissa could be plotted as single lines. Comparison of experimental data with these curves as presented in this report and other reports showed reasonable agreement for short bearings.

The resulting solution applied best to bearings having a length-diameter ratio up to about 1 and may be called the "short-bearing approximation." It yields simplified relationships including oil flow and the effect of length-diameter ratio. The curves for short bearings as developed in this report were compared with the theoretical curves of Sommerfeld and Cameron and Wood. Conclusions were reached indicating that this approximation is of practical value for analysis of bearings of small length-diameter ratio.

INTRODUCTION

For more than a half century, investigators of the problems of lubrication have offered analytical solutions giving the distribution of pressure in the oil film of slider and journal (cylindrical) bearings under load. Most investigators have based their functions on exact or approximate mathematical solutions of Reynolds' equation (reference 1):

$$\frac{\partial}{\partial x}\left(h^3 \frac{\partial p}{\partial x}\right) + \frac{\partial}{\partial z}\left(h^3 \frac{\partial p}{\partial z}\right) = 6\mu U \frac{\partial h}{\partial x} \tag{1}$$

Michell, Kingsbury, and Christopherson have presented solutions which may be considered exact in that such solutions satisfy Reynolds' equation for certain finite shapes of bearing surfaces supporting a central normal load. Michell (reference 2) solved equation (1) mathematically for the rectangular slider bearing. Kingsbury (reference 3) determined the pressure distribution of finite slider bearings and of finite journal bearings satisfying equation (1) by an experimental electrical analogy. Christopherson (reference 4) determined the pressure in journal bearings of finite length by utilizing the mathematical method of "relaxation." Cameron and Wood (reference 5) have extended the work of Christopherson to show the effect of length-diameter ratio on eccentricity ratio, attitude angle, and friction coefficient. In all cases, these solutions are given to express natural phenomena in the oil film on the basis of Reynolds' assumptions regarding lubrication, the most important assumption being that certain terms in the generalized Navier-Stokes equations (references 6 and 7) for flow in a viscous fluid may be neglected.

Some solutions of Reynolds' equation, often termed approximate solutions, have been realized by considering either the second term or the first term of the left side of equation (1) equal to zero. Such solutions for pressure distribution give considerably simplified mathematical relationships among the variables. They are exact solutions in the sense that they satisfy equation (1) for the case of a bearing of infinite axial length, on the one hand, and for the infinitely short bearing, on the other. However, they are regarded as approximate solutions when used to determine the pressure distribution in bearings of finite length.

Sommerfeld (reference 8) and Harrison (reference 9) evolved a solution for journal bearings by assuming $\partial p/\partial z = 0$, thus eliminating the second of the left-hand terms of equation (1). Such an assumption states

that there is no endwise flow as in the case of an infinitely long bearing or the case of a finite bearing in which end leakage is prevented.

Michell (reference 10), who solved equation (1) for the rectangular slider bearing, suggested a solution for the journal bearing by dropping the first of the left-hand terms in Reynolds' equation. Cardullo (reference 11) also presented this solution as giving the pressure distribution in journal bearings of finite lengths usually found in engineering practice. Because the solution by these investigators attaches great importance to the endwise flow, it has been generally regarded as applying to the case of an infinitely short bearing in which an appreciable endwise flow exists because of the absence of much resistance to such flow. It is perhaps because of this assumption that analytical work was not extended beyond the development of a pressure-distribution function.

At first thought, it would seem that dropping the first term in Reynolds' equation assumes that the pressure gradient in the circumferential direction is zero, thus making any solution on this basis useless. However, as indicated in the detailed treatment in this report, this assumption may be interpreted, not as giving a zero circumferential pressure gradient, but as giving a finite gradient whose effect on the circumferential flow of a short bearing is small compared with the effect of changing film thickness. The effect of the circumferential gradient on the flow is intimately connected with the axial pressure gradient and the shape of the bearing as given by the length l and the diameter d. Both gradients depend upon the distance from the point of maximum film pressure to a boundary where the pressure is zero. These distances are related to $\pi d/4$ for the circumferential gradient and $l/2$ for the axial gradient. Thus, as l becomes small compared with d, the circumferential gradient becomes small compared with the axial gradient.

Reliable experimental measurements of pressure distribution in finite journal bearings were obtained by McKee and McKee (reference 12) sometime after the mathematical treatments of Michell and Cardullo were published and discussed. On comparison, it was shown that the theoretical Sommerfeld-Harrison distribution was not in agreement with experimental data. Bradford and Grunder (reference 13), after conducting experiments, also demonstrated that the Harrison theory did not agree for finite cases. Almost no effort was made to compare the Michell-Cardullo theory with the experiments although a comment was made by Hersey in reference 12 that Rouse had found the Michell-Cardullo theory to be in better agreement with experiment than was the Sommerfeld-Harrison theory.

This report concerns the extension of the short-bearing pressure-distribution function of Michell and Cardullo to give equations for the

various bearing characteristics. This short-bearing approximation makes available formulas relating eccentricity ratio to applied load, attitude angle, angular position of peak film pressure, friction, required oil flow, and the ratio of peak film pressure to unit pressure on projected area.

Experimental oil film pressure data obtained by DuBois, Mabie, and Ocvirk (reference 14) indicate that the short-bearing pressure-distribution function is in reasonable agreement with natural phenomena in a high-speed, heavily loaded journal bearing of $l/d = 1.0$. Experimental data by McKee and McKee (reference 12) also show this function to be in reasonable agreement for low-speed, lightly loaded bearings of $l/d = 1.15$. Comparisons of experimental and analytical pressure distributions are shown in the figures of this report. Another experimental report (reference 15) shows the extent of the agreement between the short-bearing approximation and experiment for bearing performance characteristics such as eccentricity ratio, attitude angle, friction, and oil flow of short bearings for l/d of 1/4, 1/2, and 1.0.

The author is greatly indebted to Professor George B. DuBois for his many helpful suggestions, especially for a suggestion which led to the recognition of the capacity number and for pointing out its fundamental characteristics.

The work reported herein is a part of a bearing research project which is being conducted at Cornell University under the sponsorship and with the financial assistance of the National Advisory Committee for Aeronautics.

SYMBOLS

Dimensional quantities:

l	bearing length, inches
d	bearing diameter, inches
r	bearing radius, inches
c_r	radial clearance, inches
c_d	diametral clearance, inches $(2c_r)$
e	eccentricity of journal and bearing axes, inches

F	circumferential bearing friction force, pounds
h	fluid film thickness, inches
u, v, w	local fluid film velocities in x-, y-, and z-directions, inches per second
U	surface speed of journal, inches per second
N	journal speed, rpm
N'	journal speed, rps
θ_{max}	angle measured from location of maximum film thickness to location of peak film pressure, degrees
α	angle measured from load line to location of peak film pressure, degrees
ϕ	attitude angle, angle between load line and line of centers of journal and bearing, degrees
P	applied central load, pounds
P_X, P_Y	components of applied load parallel and normal to line of centers of journal and bearing, pounds
p	local fluid film pressure, pounds per square inch
p_o	pressure at $\theta = 0$ and π in theory of bearing without endwise flow, pounds per square inch
p_{max}	peak pressure in fluid film, pounds per square inch
p'	unit pressure on projected area, pounds per square inch
τ_x, τ_z	fluid shearing stress in x- and z-directions, pounds per square inch
q_x, q_z	flow per unit time in x- and z-directions, cubic inches per second
Q	rate of oil flow, cubic inches per second
Q_{req}	required rate of fluid flow, cubic inches per second
μ	absolute viscosity of fluid, reyns $\left(\frac{\text{Centipoises}}{6.9 \times 10^6}\right)$

Nondimensional quantities:

n	eccentricity ratio or attitude $\left(\frac{e}{c_r}\right)$
c_r/r	radial clearance ratio
c_d/d	diametral clearance ratio
l/d	length-diameter ratio
C_n	capacity number $\left(S\left(\frac{l}{d}\right)^2 = \frac{\mu N'}{p'}\left(\frac{d}{c_d}\right)^2\left(\frac{l}{d}\right)^2\right)$
S	Sommerfeld number $\left(\frac{\mu N'}{p'}\left(\frac{d}{c_d}\right)^2\right)$
f	friction coefficient $\left(\frac{F}{P}\right)$
f_v	friction variable $\left(f\left(\frac{d}{c_d}\right)\left(\frac{l}{d}\right)^2\right)$
q_n	required oil flow number $\left(\frac{Q_{req}}{\pi d l c_d \frac{N'}{2}}\right)$
k	peak-pressure ratio $\left(\frac{p_{max}}{p'}\right)$

PRESSURE DISTRIBUTION IN SHORT JOURNAL BEARINGS UNDER NORMAL CENTRAL LOAD

The early portion of the following analysis embodies the assumption and analytical reasoning employed by Reynolds (reference 1) to yield equation (1).

Analysis Following Reynolds' Method

When acted upon by a normal central load, the rotating journal is made to displace with respect to the stationary bearing such that the element of fluid dx, dy, and dz of figure 1 moves in a converging film of oil. Because the fluid is viscous, the rotating journal causes the element to flow into the wedge at a circumferential velocity u; since the oil film is of finite extent in the axial direction of the bearing, the element has a velocity w in the endwise direction.

Both bearing and journal are of length l and diameter d or radius r. The journal rotates at a constant angular velocity having a surface velocity of U with respect to the stationary bearing surface. Because the centers of the bearing O and the journal O' are displaced by an amount e, the oil film will be of variable thickness h. It is assumed that the circumferential dimension of the film may be unwrapped such that oil film is essentially moving between surfaces one of which may be considered a plane. The coordinates x, y, and z are chosen as shown in figure 1 such that the x-direction is circumferential, the y-direction is radial, and the z-direction is measured from the center of the bearing parallel to the bearing and journal axes.

Figure 2 shows the forces which are assumed to act on the fluid element in laminar flow at an arbitrary location in the converging oil film. In both x- and z-directions, it is assumed that shearing stresses τ_x and τ_z and normal pressures p are acting as shown. In the x-direction, for example, two shearing vectors and two normal vectors are assumed; in the general case, two additional shearing vectors should be shown acting on the sides of the element, but these are considered negligible.

Assuming that static equilibrium of an incompressible fluid prevails and that inertia forces are negligible, the summation of forces in the x-direction and separately in the z-direction result in the following relationships between shearing and normal pressures. In the following, because of similar mathematical treatment, equations applying in the z-direction are developed in parallel with equations in the x-direction. Thus

$$\frac{\partial \tau_x}{\partial y} = \frac{\partial p}{\partial x} \tag{2}$$

$$\frac{\partial \tau_z}{\partial y} = \frac{\partial p}{\partial z} \tag{2a}$$

The shearing stress acting between layers of viscous fluid in laminar flow is dependent upon the inverse slope of the velocity profile as given below:

$$\tau_x = \mu \frac{\partial u}{\partial y} \tag{3}$$

$$\tau_z = \mu \frac{\partial w}{\partial y} \tag{3a}$$

where μ is the absolute viscosity of the fluid.

Differentiating equations (3) and (3a) with respect to y and substituting in equations (2) and (2a) give:

$$\mu \frac{\partial^2 u}{\partial y^2} = \frac{\partial p}{\partial x} \tag{4}$$

$$\mu \frac{\partial^2 w}{\partial y^2} = \frac{\partial p}{\partial z} \tag{4a}$$

Equations (4) and (4a) are integrated to give variations of velocities u and w with respect to y throughout the thickness of the oil film (velocity profiles) by assuming that the viscosity and pressure are constant throughout the oil film thickness. Thus, μ, $\partial p/\partial x$, and $\partial p/\partial z$ are constants with respect to y. Assuming that no slip exists between fluid and bearing surfaces, the boundary conditions are: $u = 0$ and $w = 0$ at $y = 0$; $u = U$ and $w = 0$ at $y = h$. Integrating equations (4) and (4a) yields:

$$u = \frac{Uy}{h} + \frac{1}{2\mu} \frac{\partial p}{\partial x} y(y - h) \tag{5}$$

$$w = \frac{1}{2\mu} \frac{\partial p}{\partial z} y(y - h) \tag{5a}$$

The forms of equations (5) and (5a) show that the velocity profiles are parabolic. It may be seen that for the velocity profile in the

circumferential direction the first term of equation (5) gives a linear velocity profile indicated by the dashed line in figure 3, and the second term makes the profile parabolic.

The velocity profiles may be used to determine the quantities of fluid flow per unit of time in the x- and z-directions. The quantity q_x is the flow in the x-direction through a transverse plane having the area $h\,dz$; the quantity q_z is the flow in the z-direction through an area $h\,dx$ as shown in figure 4. These quantities may be expressed as follows:

$$q_x = \int_0^h u\,dy\,dz = \left(\frac{Uh}{2} - \frac{h^3}{12\mu}\frac{\partial p}{\partial x}\right)dz \tag{6}$$

$$q_z = \int_0^h w\,dy\,dx = \left(-\frac{h^3}{12\mu}\frac{\partial p}{\partial z}\right)dx \tag{6a}$$

Considering the flow of fluid through an elemental volume of dimensions h, dx, and dz as shown in figure 5, an equation of continuity of flow may be written since it is required that the quantity entering must be equal to the quantity leaving. A steady state of flow is assumed. Thus,

$$q_x + q_z = q_x + \frac{\partial q_x}{\partial x}dx + q_z + \frac{\partial q_z}{\partial z}dz$$

$$\frac{\partial q_x}{\partial x}dx + \frac{\partial q_z}{\partial z}dz = 0 \tag{7}$$

Equation (7) indicates that the rate of increase in flow in one direction is equal to the decrease in the rate of flow in the other direction. Substituting in equation (7) the proper derivatives of equations (6) and (6a) and assuming that the viscosity is constant in all regions of the fluid result in Reynolds' equation in the form of equation (1).

Principal Assumption for Short Bearings

The following analysis results in the pressure-distribution function as given by Michell and Cardullo. The principal simplifying

assumption made in this analysis is one regarding equation (6) for the flow in the x-direction, namely, that, of the two right-hand terms, the second is negligible compared with the first. Referring to figure 3(a), the first term represents the flow as given by the area of the triangular portion of the velocity profile; the area of the profile between the dashed line and the parabolic curve is considered to be small by comparison. This does not mean that $\partial p/\partial x$ is necessarily small, but that the term $h^3/12\mu(\partial p/\partial x)$ is small. Thus, it is assumed that:

$$q_x = \frac{Uh}{2}\,dz \tag{8}$$

Comparing equation (8) with equation (6), it may be seen that the assumption made results eventually in the omission of the first of the left-hand terms in Reynolds' equation (equation (1)). The solution which follows will therefore include that part of the circumferential flow proportional to journal surface velocity and varying film thickness but will neglect the effect of circumferential pressure gradient on this flow. Any change in circumferential flow will directly influence the axial flow and the axial pressure gradient.

The shape of the bearing as given by the length l and the diameter d affects the relationship between the circumferential and axial pressure gradients. Both gradients depend upon the distance from the point of maximum film pressure to a boundary where the pressure is zero. For the circumferential gradient this distance is related to $\pi d/4$ and is related to $l/2$ for the axial gradient. Thus, as l becomes small compared with d, the circumferential gradient becomes small compared with the axial gradient.

Neglecting the effect of circumferential pressure gradient on the flow, the rates of change of flow in the x- and z-directions are given by differentiating equations (8) and (6a):

$$\frac{\partial q_x}{\partial x} = \frac{U}{2}\frac{\partial h}{\partial x}\,dz \tag{9}$$

$$\frac{\partial q_z}{\partial z} = \frac{\partial}{\partial z}\left(-\frac{h^3}{12\mu}\frac{\partial p}{\partial z}\right)dx \tag{9a}$$

Equation (9) is a result of the above assumption and indicates that, when the flow is into the converging oil film, the decrease in

flow in the circumferential direction is due primarily to a decrease in film thickness. Substituting equations (9) and (9a) in the continuity equation (7) results in the simple differential equation:

$$\frac{\partial}{\partial z}\left(\frac{h^3}{12\mu}\frac{\partial p}{\partial z}\right) = \frac{U}{2}\frac{\partial h}{\partial x}$$

$$\frac{\partial}{\partial z}\left(h^3\frac{\partial p}{\partial z}\right) = 6\mu U\frac{\partial h}{\partial x} \tag{10}$$

Referring to Reynolds' equation (equation (1)) it is seen that equation (10) lacks the first left-hand term. Since h is not a function of z, equation (10) may be written:

$$\frac{d^2p}{dz^2} = \frac{6\mu U}{h^3}\frac{dh}{dx} \tag{10a}$$

Further, since none of the terms on the right-hand side of equation (10a) are functions of z, integration gives:

$$\frac{dp}{dz} = \frac{6\mu U}{h^3}\frac{dh}{dx}z + C_1$$

$$p = \frac{6\mu U}{h^3}\frac{dh}{dx}\frac{z^2}{2} + C_1 z + C_2$$

The constant of integration C_1 may be evaluated from the boundary condition that $dp/dz = 0$ at $z = 0$ for symmetrical flow about the transverse plane of symmetry at the center of the bearing. From the condition that pressures at the ends of the bearing are at the atmospheric datum of zero gage pressure, C_2 may be determined from $p = 0$ at $z = \pm l/2$. Thus the pressure distribution as a function of x and z is given by:

$$p = \frac{3\mu U}{h^3}\frac{dh}{dx}\left(z^2 - \frac{l^2}{4}\right) \tag{11}$$

Since $dx = r\,d\theta$, equation (11) may be given in polar coordinates:

$$p = \frac{3\mu U}{rh^3}\frac{dh}{d\theta}\left(z^2 - \frac{l^2}{4}\right) \tag{11a}$$

For the journal axis displaced e with respect to the bearing axis, the film thickness may be approximated by:

$$h = c_r + e\cos\theta = c_r(1 + n\cos\theta) \tag{12}$$

where c_r is the radial clearance and n is the eccentricity ratio, or attitude of the journal with respect to bearing, given by the ratio e/c_r. As shown in figure 1, θ is measured from the station where the the film is of maximum thickness. Thus

$$\frac{dh}{d\theta} = -c_r n\sin\theta \tag{12a}$$

Substituting equations (12) and (12a) in equation (11a):

$$p = \frac{3\mu U}{rc_r^2}\left(\frac{l^2}{4} - z^2\right)\frac{n\sin\theta}{(1 + n\cos\theta)^3} \tag{13}$$

Expression (13) shows that the pressure distribution is parabolic in the z-direction and sinusoidal in the circumferential direction giving zero pressures at $z = \pm l/2$ and $\theta = m\pi$ where m is an integer. Figure 6 shows the approximate forms of the distributions in the x- and z-directions.

EXTENSION OF ANALYSIS RESULTING IN BEARING PERFORMANCE CHARACTERISTICS

As discussed in another section of this report, experimental data show that the pressure-distribution function as given by equation (13)

is in good agreement with short-journal-bearing behavior. This apparent agreement has led to the extension of the analysis to include the determination of other bearing characteristics, given below, which the pressure-distribution function makes possible.

Extent of Pressure in Full Cylindrical Bearings

As shown in figure 6 the circumferential pressure distribution given by equation (13) is positive in the converging film $0 < \theta < \pi$ and is negative in the diverging film $\pi < \theta < 2\pi$. The maximum negative pressure is shown to be equal in magnitude to the maximum positive pressure, a condition which does not appear to exist except in very lightly loaded bearings. A negative pressure of small magnitude, as shown by the dashed line in figure 6, not exceeding that of atmospheric pressure, is possible. In the absence of a high datum pressure, the negative pressures are assumed to be of negligible magnitude. It is assumed, for moderately and heavily loaded bearings, that the positive pressure region from $\theta = 0$ to π, as given by equation (13), carries the total load.

Applied Load P and Capacity Number C_n

The external load P may be related to pressures induced in the oil film by performing certain integrations. Choosing X- and Y-axes as shown in figure 7, the integrations of pressures on the journal in the directions of these axes will give components P_X and P_Y of the resultant force which is equal to P. The integral expressions for P_X and P_Y are:

$$P_X = -2\int_0^{\pi}\int_0^{l/2} pr \cos\theta \, d\theta \, dz$$

$$P_Y = 2\int_0^{\pi}\int_0^{l/2} pr \sin\theta \, d\theta \, dz$$

Substituting equation (13) for p and integrating with respect to z:

$$P_X = -\frac{\mu U l^3}{2c_r^2}\int_0^{\pi} \frac{n \sin\theta \cos\theta \, d\theta}{(1 + n\cos\theta)^3} \qquad (14)$$

$$P_Y = \frac{\mu U l^3}{2c_r^2} \int_0^{\pi} \frac{n \sin^2\theta \, d\theta}{(1 + n \cos \theta)^3} \tag{14a}$$

Employing Sommerfeld's mathematical technique (see appendix), the integrations with respect to θ yield:

$$P_X = \frac{\mu U l^3}{c_r^2} \frac{n^2}{(1 - n^2)^2} \tag{15}$$

$$P_Y = \frac{\mu U l^3}{4c_r^2} \frac{\pi n}{(1 - n^2)^{3/2}} \tag{15a}$$

The applied load is given by:

$$P = \sqrt{P_X^2 + P_Y^2}$$

$$= \frac{\mu U l^3}{4c_r^2} \frac{n}{(1 - n^2)^2} \left[\pi^2(1 - n^2) + 16n^2\right]^{1/2} \tag{16}$$

Substituting $P = p' l d$ and $U = \pi N' d$ gives:

$$\frac{\mu N'}{p'} \left(\frac{d}{c_d}\right)^2 \left(\frac{l}{d}\right)^2 = \frac{(1 - n^2)^2}{\pi n} \left[\frac{1}{\pi^2(1 - n^2) + 16n^2}\right]^{1/2}$$

The left-hand term is a grouping of bearing variables in nondimensional form and is seen to be dependent upon the eccentricity ratio, or attitude, n. This term is the capacity number C_n and may be recognized as the Sommerfeld number S times the square of the length-diameter ratio. Thus,

$$C_n = S\left(\frac{l}{d}\right)^2 = \frac{(1 - n^2)^2}{\pi n} \left[\frac{1}{\pi^2(1 - n^2) + 16n^2}\right]^{1/2} \tag{17}$$

Attitude Angle ϕ

The angular position of the line of action of the load P with respect to the location of the minimum film thickness, or point of closest approach, is the attitude angle ϕ, as shown in figure 7, which may be determined from:

$$\tan \phi = \frac{P_Y}{P_X}$$

$$= \frac{\pi}{4} \frac{\left(1 - n^2\right)^{1/2}}{n} \tag{18}$$

Figure 8 shows the journal bearing reoriented such that the load line of action is vertical.

Peak-Pressure Angle α

The angular position of the location of peak pressure with respect to the load line is the peak-pressure angle α as shown in figure 8. By determining θ_{max}, the angle at which maximum pressure acts, α may be determined. Differentiating equation (13) with respect to θ and maximizing:

$$\theta_{max} = \cos^{-1}\left[\frac{1}{4n}\left(1 - \sqrt{1 + 24h^2}\right)\right] \tag{19}$$

$$\alpha = \phi - \left(180 - \theta_{max}\right) \tag{20}$$

Friction Variable f_v

Because of the assumed linear velocity profile in the oil film in the circumferential direction, the shearing stress at any location θ is the same at both the journal surface and the bearing surface and may be expressed as:

$$\tau_x = \mu \frac{\partial u}{\partial y}$$

$$= \mu \frac{U}{h}$$

The circumferential friction force may be evaluated by the following integral:

$$F = \int_0^{2\pi} \tau_x l r \, d\theta$$

$$= \int_0^{2\pi} \mu \frac{U}{h} l r \, d\theta$$

With $h = c_r(1 + n \cos \theta)$, then

$$F = \frac{\mu U l r}{c_r} \int_0^{2\pi} \frac{d\theta}{(1 + n \cos \theta)}$$

$$= \frac{\mu U l r}{c_r} \frac{2\pi}{(1 - n^2)^{1/2}}$$

The coefficient of friction f is commonly defined as the ratio of friction force to the applied load.

$$f = \frac{F}{P}$$

$$= \frac{\mu U l r}{P c_r} \frac{2\pi}{(1 - n^2)^{1/2}}$$

$$f\left(\frac{r}{c_r}\right)\left(\frac{l}{d}\right)^2 = \frac{\mu N'}{p'}\left(\frac{r}{c_r}\right)^2\left(\frac{l}{d}\right)^2 \frac{2\pi^2}{(1 - n^2)^{1/2}}$$

$$f_v = f\left(\frac{d}{c_d}\right)\left(\frac{l}{d}\right)^2$$

$$= C_n \frac{2\pi^2}{(1 - n^2)^{1/2}}$$

The first equivalent of f_v in equation (21) is the friction variable representing a nondimensional grouping of bearing variables including the coefficient of friction. The friction variable is basically dependent upon the eccentricity ratio as indicated by the last equivalent which also includes the capacity number.

Oil Flow Number q_n

Equation (6a) may be used to determine the rate of oil flow discharging from the two ends of the bearing. Proper substitution for h and dp/dz gives the following expression for the axial flow at any point in the oil film:

$$q_z = \frac{Uc_r nz}{2} \sin \theta \, d\theta$$

At the ends of the bearing:

$$q_{z=\pm l/2} = \pm \frac{Uc_r nl}{4} \sin \theta \, d\theta$$

The above equations indicate that the axial flow will be outward from the bearing in the region of the converging film $0 < \theta < \pi$ where the pressures are positive. They also show that in order to develop negative pressures in the film at $\pi < \theta < 2\pi$, the oil flow must be axially inward. A reservoir of fluid must be available at the ends of the bearing as a source of supply. The rate of outward axial oil flow Q at the ends of the bearing from the region of positive pressure is given by the following integral:

$$Q = 2 \int_0^{\pi} \frac{Uc_r nl}{4} \sin \theta \, d\theta$$

$$= Uc_r ln$$

$$= \pi dlc_d \frac{N'}{2} n \qquad (22)$$

Equation (22) gives the flow which is the result of hydrodynamic action of the load-carrying film, and it is seen to depend upon the eccentricity ratio n. The rate of flow to be supplied to the bearing through an inlet hole or grooves on the unloaded side of the bearing must be equal to that given by equation (22) which may be looked upon as the required rate of flow. Equation (22) in the following non-dimensional form is the required oil flow number:

$$q_n = \frac{Q_{req}}{\pi d l c_d \frac{N'}{2}} = n \tag{23}$$

The required oil flow number is seen to be numerically equal to the eccentricity ratio.

Peak-Pressure Ratio k

The ratio k of peak pressure in the oil film to the unit pressure, where the unit pressure p' is defined as the load divided by the projected area of the bearing, is termed peak-pressure ratio. Since θ_{max} is known, it is seen that the peak pressure is given at z = 0 as:

$$p_{max} = \frac{3\mu U l^2}{4rc_r^2}\left[\frac{n \sin \theta_{max}}{(1 + n \cos \theta_{max})^3}\right]$$

Therefore,

$$k = \frac{p_{max}}{p'}$$

or

$$k = C_n \frac{6\pi n \sin \theta_{max}}{(1 + n \cos \theta_{max})^3} \tag{24}$$

CURVES FOR SHORT JOURNAL BEARINGS

As shown in figure 9, the manner in which the film pressures are distributed in the circumferential direction is dependent upon the trigonometric portion of equation (13) which has been termed the

pressure-distribution function. It may be seen that the interesting region of the distribution is in the second quarter of the converging oil film for $\pi/2 < \theta < \pi$ where the pressures and pressure gradients become great for large values of the eccentricity ratio; for $n = 1.0$ the maximum pressure approaches an infinite value since the denominator of equation (13) becomes zero at $\theta = \pi$. The locus of peak values of the distribution function shows that the maximum pressure is at $\theta = \pi/2$ for $n = 0$ and moves to the location of minimum film thickness at $\theta = \pi$ for $n = 1.0$. The curve of figure 9 indicates that theoretically extremely high pressures may be sustained by the hydrodynamic action of the lubricant without metallic contact of the bearing surfaces; in practice, this is limited by the exactness of the bearing surfaces, freedom of the lubricant from dirt and grit, the strength of the materials of the bearing surfaces, and the rigidity of the journal and bearing against bending or other elastic deformations.

The form of equation (13) for short bearings may be compared with the following distribution function as given by Sommerfeld for bearings without endwise flow:

$$p = \frac{\mu U r}{c_r^2}\left[\frac{6n(2 + n \cos \theta) \sin \theta}{(2 + n^2)(1 + n \cos \theta)^2}\right] + p_o \qquad (25)$$

where p_o is the datum pressure at $\theta = 0$ and π (maximum and minimum film thickness) which may be calculated from the pressure at the location where the fluid enters the bearings, usually taken at $\theta = 3/2\pi$. For $p_o = 0$, equation (25) gives negative pressures of magnitude equal to the positive pressures.

Attitude Angle ϕ

As shown in the polar diagram of figure 10, the attitude angle is plotted as a function of the eccentricity ratio from equation (18). The attitude angle gives the angular position of the line through the bearing and journal centers with respect to the line of action of the applied load. At values of n near zero, the line of centers is nearly normal to the load line and becomes parallel to the load line at $n = 1.0$. The general shape of the path of the journal center shown has been given by other investigators both analytically and experimentally. Bradford and Davenport (reference 16) have obtained an experimental curve whose shape is similar to the curve of figure 10. As may be seen, the path of the journal is slightly within a semicircle.

Capacity Number C_n

The equations given in the foregoing sections show that the quantities representing bearing behavior are dependent upon eccentricity ratio. The capacity number is also related to the eccentricity ratio. Thus, curves are presented showing short-bearing performance plotted as a function of the capacity number for simplicity and usefulness, as C_n is easily determined. Equation (17) gives the required relationship between capacity number and eccentricity ratio such that peak-pressure angle, friction variable, required oil flow number, and peak-pressure ratio as well as eccentricity ratio may be plotted as functions of the capacity number as shown in figures 11 to 15.

Customarily eccentricity ratio and friction variable have been plotted as functions of the Sommerfeld number in which single-line curves give values for bearings without endwise flow. Recently, for bearings having endwise flow (reference 5), families of curves on the basis of Sommerfeld number have been given with length-diameter ratio as a parameter.

Because the capacity number includes both the Sommerfeld number and the square of the length-diameter ratio, the curves of figures 11 to 15 appear as single lines. To illustrate the basic role of the capacity number, the same performance quantities are shown plotted against Sommerfeld number in figures 16 to 20.

Eccentricity ratio n as a function of capacity number C_n is given by the curve of figure 11. As in the case of pressure distribution, it may be seen that extremely heavy loads may theoretically be supported by the oil film at large values of the eccentricity ratio. An infinite load is theoretically required at $n = 1.0$ for metallic contact of the bearing surfaces. Figure 16 shows the family of curves which result from plotting eccentricity ratio n as a function of the Sommerfeld number S. It may be seen that for a given eccentricity ratio, the load capacity increases as the square of the length-diameter ratio increases within the l/d range of short bearings.

The curve of figure 12, based on equations (17) to (20), shows the manner in which the angular position α of peak pressure in the oil film varies with capacity number. The peak pressure is shown to be at the load line for $n = 1.0$; although it is not shown, the location of the peak pressure also approaches the load line as n approaches zero. An interesting feature is that the maximum angular displacement of the peak pressure as given by α is approximately 20° at $n \approx 0.4$ and $C_n \approx 0.15$. For comparison, if the extent of the oil film is considered to be 2π, as in the Sommerfeld solution, the value of α reaches a maximum of 90° at $n = 1.0$. Figure 17 gives the values of α in figure 12 as a family of curves plotted with Sommerfeld number as abscissa.

As obtained from equations (21) and (17), the friction variable as a function of capacity number is shown in figure 13 and as a function of Sommerfeld number in figure 18. The nondimensional forms of the friction variable in the two figures differ in that, as given in figure 13, the friction variable includes the square of the length-diameter ratio whereas, in figure 18, it is in the form originally given by Sommerfeld. Theoretically, no distinction can be made between friction variable for the bearing and that for the journal inasmuch as the velocity profile in the oil film is assumed to be linear. Actually, a difference is thought to exist which depends upon the couple equal to $Pe \sin \phi$. In figure 18, it appears that for l/d ratios greater than 1.0 the curves of friction variable would approach the straight line given by Petroff.

It is interesting to note from equation (23) that the oil flow number corresponding to the flow required in the loaded portion of the film is numerically equal to the eccentricity ratio n. Therefore, the curve in figure 14 of required oil flow number against capacity number is identical with the curve of eccentricity ratio in figure 11. Similarly, the curves in figures 19 and 16 are numerically identical. Although the curves are not extended to give values at $n = 0$, it may be shown that no oil flow is required for zero load and $n = 0$.

Equation (24) gives the curve of peak-pressure ratio as a function of capacity number in figure 15. Plotted against the Sommerfeld number, the curves of peak-pressure ratio appear as in figure 20. For the region of low applied loads in figure 15, k is approximately 2.0 and rises rapidly to an infinite value as the capacity number approaches zero and n approaches 1.0.

COMPARISON OF EXPERIMENT WITH THEORY

Experimental measurements of oil film pressure distributions in short bearings were obtained from references 12 and 14. These were compared with the pressure distributions given by equation (13) as shown in figures 21 to 25.

Measurements of bearing characteristics such as eccentricity ratio, attitude angle, friction variable, and oil flow number are given in reference 15 where comparisons are shown with the analytical values obtained from the equations and curves of this report. These measurements indicate that the short-bearing theory is in good agreement with experiment for bearings having length-diameter ratios of 1/4, 1/2 and 1.

Comparison with Model 2

A number of plaster models pictured in reference 14 show the measured oil film pressures in a full journal bearing with babbit lining. Model 2 of the group of five models represents the pressure distribution for a bearing of $l/d = 1.0$ acted upon by a normal central load. Model 2 alone is of interest since the other models represent measured pressures for bearings acted upon by misalined loads and moments.

The measured circumferential pressure distributions as shown in model 2 are given by the solid lines of figure 21. Circumferential pressures at the center of the $1\frac{5}{8}$- inch-long bearing and at 1/4, 1/2, and 3/4 inch on each side of center are shown. The plotting of experimentally measured pressures is such that the angle at the load line is 90°.

The following data represent the conditions which prevailed in taking film pressure data for model 2:

Bearing diameter, d, in.	$1\frac{5}{8}$
Bearing length, l, in.	$1\frac{5}{8}$
Load, P, lb	2200
Bearing pressure on projected area, p', lb/sq in.	833
Speed, N, rpm	5000
N', rps	83.3
Average film temperature, °F	197
Absolute viscosity at 197° F, 16.7 centipoises or μ in reyns	2.42×10^{-6}
Diametral clearance at room temperature, in.	0.0033
Diametral clearance at 197° F, in.	0.0020
Radial clearance at 197° F, in.	0.0010

Aviation 1120 oil was preheated to 140° F and pumped into the bearing at a pump pressure of 40 pounds per square inch; the oil entered the bearing at the center through two 1/8-inch-diameter holes, 45° apart, on the unloaded side of the bearing. The viscosity of the oil given above is based on the bearing temperature given by a thermocouple located 1/16 inch from the bearing surface at the center of the bearing on the loaded side.

In order to calculate the analytical values from equation (13) for the above conditions, the eccentricity ratio is first determined from the capacity number and the curve of figure 11. Thus,

$$C_n = \frac{\mu N'}{p'}\left(\frac{d}{c_d}\right)^2\left(\frac{l}{d}\right)^2$$

$$= \frac{2.42 \times 10^{-6} \times 83.3}{833}\left(\frac{1.625}{0.002}\right)^2(1)^2$$

$$= 0.159$$

and, in accordance with figure 11,

$$n = 0.415$$

The analytical pressure-distribution curves given as the short-bearing-theory curves of figure 21 were determined from equation (13) for $n = 0.415$ and $z = 0, \pm 1/4, \pm 1/2$, and $\pm 3/4$ inch as follows:

$$p = \frac{3\mu U}{rc_r^2}\left(\frac{l^2}{4} - z^2\right)\frac{n \sin \theta}{(1 + n \cos \theta)^3}$$

$$= 3790\left(\frac{l^2}{4} - z^2\right)\frac{0.415 \sin \theta}{(1 + 0.415 \cos \theta)^3}$$

Since the angular scale θ is different from the scale used in the experiment, two angular scales are required differing by $90^\circ - \phi$.

From the analytical values of C_n and n above, the following quantities are determined from the curves of figures 10, 12, and 15: Attitude angle, peak-pressure angle, and peak-pressure ratio, respectively. These are compared below with the experimental quantities taken from model 2.

Quantity	Experimental	Analytical
Attitude angle,[1] ϕ, deg	60	60
Peak-pressure angle, α, deg	20	$19\frac{1}{2}$
Peak-pressure ratio, k	2.49	2.50

[1]Analytical value of ϕ is measured from load line to location of zero pressure which theoretically coincides with minimum film thickness.

Figure 21 shows that the analytical and experimental distributions are in reasonably good agreement except in the region of closest approach near the ends of the bearing. It is believed that if the bearing surfaces were exactly cylindrical, and without elastic deformation, the experimental curves would meet commonly at the position of closest approach as shown by the theoretical curves. The actual position of closest approach may be variable along the length of the bearing because of deflection and bellmouthing.

The experimental curves of model 2 are the averages of pressures taken for clockwise and counterclockwise rotation of the journal; also, they are averages of pressures at corresponding points each side of the central transverse plane of the bearing, as indicated in reference 14. The pressures of model 2 were measured over an angular range of approximately 180° so that it is not possible to compare the theoretical distribution function over the full 180°. However, as shown, the comparison is made in the important higher-pressure range.

In the calculation of capacity number, it may be seen that the determination of the bearing clearance at operating film temperature is of critical importance; using the room-temperature clearance would result in a much larger eccentricity ratio. Figure 26 gives the changes in diametral clearance as a function of the operating film temperature of the test bearing used to obtain data for model 2. This curve was determined experimentally by slowly increasing the speed of the journal and thereby increasing the film temperature to the point where the differential expansion of the journal and bearing caused incipient seizure of the parts. At seizure, the room-temperature clearance is reduced to zero, giving a measure of the change in clearance as a function of film temperature. As is shown in figure 26, two seizure points and conditions at room temperature give three points to determine the curve.

Curves of circumferential pressure distribution as given analytically by Sommerfeld's solution for bearings having no endwise flow are also shown in figure 21. The eccentricity ratio as given by the following equation is $n = 0.106$ for the conditions of model 2:

$$S = \frac{\mu N'}{p'}\left(\frac{d}{c_d}\right)^2 = \frac{(2 + n^2)\sqrt{1 - n^2}}{12\pi^2 n} \tag{26}$$

It may be seen that the eccentricity ratio determined by the Sommerfeld equation is about one-fourth of that determined by the short-bearing theory. This is a consequence primarily of assuming that the unloaded side of the bearing contributes to the support of the applied load.

Using the value of $n = 0.106$, the pressure distribution is given by equation (25). The value of p_o may be determined by taking the pressure at $\theta = 3/2\pi$ as the inlet pressure of 40 pounds per square inch. Substituting in equation (25):

$$p = -\frac{\mu U r}{c_r^2}\left(\frac{12n}{2 + n^2}\right) + p_o$$

$$p_o = \frac{2.42 \times 10^{-6} \times 2\pi \times 83.3 \times 0.812^2}{(0.001)^2}\left(\frac{12 \times 0.106}{2 + 0.0112}\right) + 40$$

$$= 570 \text{ lb/sq in.}$$

Equation (25) also gives the pressure distribution:

$$p = \frac{\mu U r}{c_r^2}\left[\frac{6n(2 + n \cos\theta) \sin\theta}{(2 + n^2)(1 + n \cos\theta)^2}\right] + p_o$$

$$= \frac{2.42 \times 10^{-6} \times 2\pi \times 83.3 \times 0.812^2}{(0.001)^2}\left[\frac{0.636(2 + 0.106 \cos\theta) \sin\theta}{(2 + 0.0112)(1 + 0.106 \cos\theta)^2}\right] + 570$$

$$= 264\left[\frac{(2 + 0.106 \cos\theta) \sin\theta}{(1 + 0.106 \cos\theta)^2}\right] + 570$$

The values of pressure from the above equation are shown plotted as a single curve in figure 21. The angular scale θ coincides with that used in the experiment because the Sommerfeld theory places the load line at $\theta = 90^\circ$.

It may be seen that the values from the short-bearing approximation are in close agreement with the experimental data presented. Comparing the two analytical solutions is not completely justified because the short-bearing theory is based on the assumption of a ruptured film

extending π degrees whereas the Sommerfeld solution is based on a complete film of 2π degrees. If the Sommerfeld case were based on a ruptured film, the eccentricity ratio would be more nearly equal to the short-bearing value. However, the pressure distributions by the two theories cannot be similar since the Sommerfeld solution gives no axial variations in film pressure.

Comparison with Experiments by McKee and McKee

Eight cases of experimental pressure distributions in bearings of $l/d = 1.15$ under normal central load are presented by McKee and McKee in reference 12. Four of the experiments were conducted on a journal bearing having a diametral clearance of 0.005 inch and four, on a bearing having 0.002-inch clearance. Both bearings were 1.00 inch long and 0.87 inch in diameter. Maximum applied loads were 25 pounds and the maximum journal speed was 592 rpm. The bearings were operated completely submerged in the lubricating oil, and the temperature of the oil was measured with a thermometer located in the oil bath several inches from the bearing film.

In figures 22 to 25, a comparison is made of the experimental distributions with those given by the short-bearing function for the four tests with the diametral clearance of 0.005 inch. The agreement between experiment and theory was better for these tests than for those with 0.002-inch diametral clearance. Calculations of capacity number, eccentricity ratio, pressure distribution, attitude angle, peak-pressure angle, and peak-pressure ratio were made in the same manner as for model 2. Some of the analytical and experimental quantities are compared in the table below.

Quantity	Test No. 1		Test No. 2		Test No. 3		Test No. 4	
	Experimental	Analytical	Experimental	Analytical	Experimental	Analytical	Experimental	Analytical
Capacity number, C_n	----	0.0815	----	0.0785	----	0.0300	----	0.0352
Eccentricity ratio, n	----	0.555	----	0.561	----	0.713	----	0.688
Attitude angle[1], ϕ, deg	50	50	48	49	52	37	$51\frac{1}{2}$	39
Peak-pressure angle, α, deg	$12\frac{1}{2}$	$18\frac{1}{2}$	12	$18\frac{1}{2}$	18	15	15	16
Peak-pressure ratio, k	3.06	3.00	3.13	3.00	3.79	3.83	2.83	3.63

[1]Analytical value of ϕ is measured from load line to location of zero pressure which theoretically coincides with minimum film thickness.

The experimental values of peak-pressure angle and peak-pressure ratio for both clearances are compared with the short-bearing analytical curves in figures 27 and 28. It may be seen that the agreement between

experiment and theory is not as close for the 0.002-inch clearance as for the larger clearance. The experimental values of peak-pressure angle in figure 27 appear to be quite divergent from the analytical values given by the curve. However, as may be seen in the pressure-distribution curves of figures 22 to 25, this divergence is less conspicuous on a different angular scale. In comparing figures 22 to 25, it may be seen that the divergence of the experimental and analytical pressures is such that the analytical values represent an average of the experimental values which are in some instances above and in some instances below the analytical ones.

Although the comparisons of the analytical quantities with those by McKee and McKee are not as close as those with model 2, it may be seen from the preceding table and figures 22 to 25 that the agreement is reasonable as to order of magnitude of pressures and the shape of the pressure-distribution curves. It is interesting to note that the region of pressures below atmospheric as shown experimentally is small enough to be considered negligible as is assumed in the short-bearing approximation.

COMPARISON OF ANALYTICAL CURVES

In both the analytical work of Cameron and Wood (reference 5) and in the short-bearing approximation of this report, length-diameter ratio has been incorporated as an important variable in journal-bearing performance. For this reason, a comparison is made in figures 29 to 31 of curves of eccentricity ratio, attitude angle, and friction variable as given by these analytical solutions. In addition, analytical curves determined by Sommerfeld (reference 8) for bearings without endwise flow are also shown for comparison.

The differences in the analytical solutions lie in the basic assumptions made in each case. Both the solutions by Cameron and Wood and the short-bearing approximation assume a ruptured film, differing from the Sommerfeld solution which assumes a continuous film of 2π degrees. This difference is of great influence as shown in the curves of eccentricity ratio and attitude angle in figures 29 and 30; the curves representing the two analytical solutions assuming ruptured films are in reasonably good agreement but are quite divergent from the solution depending upon a continuous film.

An important difference between the solution by Cameron and Wood and the short-bearing solution is that the former is based on a ruptured film whose extent depends upon the Sommerfeld number and the latter assumes that the ruptured film extends π degrees for all values of the

Sommerfeld number. Another important difference is that the solution by Cameron and Wood is exact mathematically in satisfying Reynolds' equation (equation (1)) whereas the short-bearing solution is not because of its assumption of a linear velocity profile in the circumferential direction of fluid flow. It is interesting to note that the two solutions for eccentricity ratio and attitude angle are less divergent as l/d becomes smaller and approach each other as l/d approaches zero.

Although the Sommerfeld solution, as shown in figure 29, gives low values of eccentricity ratio at the high Sommerfeld numbers, it is interesting to note that it gives higher eccentricity ratios than the short-bearing solution in the heavily loaded region of low Sommerfeld numbers. Intersections of the Sommerfeld curve with short-bearing curves represent identical conditions of load and eccentricity ratio. Apparently the Sommerfeld curve and the curves plotted by Cameron and Wood for $l/d = \infty$ do not intersect as is indicated by the two curves in figure 29.

Figure 31 compares friction variable as given by the three analytical solutions. Again the theory of Cameron and Wood and the short-bearing theory are in close agreement as to the effect of l/d ratios. Because the solution by Cameron and Wood satisfies Reynolds' equation, it shows a difference in friction variable for the bearing and for the journal as shown in figure 31; the short-bearing solution does not indicate this difference because of the assumed linear circumferential film velocity profile. For an l/d greater than 1.0, all solutions are well approximated by the Petroff line at the high Sommerfeld numbers. It is interesting that all solutions assume a 2π film in determining the friction variable although a ruptured film is assumed in two instances. Apparently this assumption is valid from the experimental results given in reference 15 and from experiments by many other investigators.

An important feature of the Sommerfeld solution and the short-bearing solution is that the solutions appear in equation form giving simple relationships among the bearing variables in nondimensional quantities such as the Sommerfeld number and the capacity number.

CONCLUSIONS

From comparisons of experimental data for film pressure distribution with the analytical values as given by the short-bearing approximation and the theoretical curves of Sommerfeld and Cameron and Wood, the following conclusions may be drawn:

1. The assumption of a linear circumferential velocity profile appears to be a good approximation of journal-bearing behavior for short bearings but a limiting length-diameter ratio to which the assumption is applicable probably exists. Experimental data on eccentricity ratio as given in NACA TN 2809 show agreement within practical limits with the analytical approximation at length-diameter ratios of 1/4, 1/2, and 1.0.

2. The assumption of a separated oil film on the unloaded side is representative of test-bearing behavior. It is interesting to note that the analytical results of Cameron and Wood and the short-bearing approximation agree on this assumption and that the resulting curves by the two analyses are in reasonable agreement in the range of low length-diameter ratios.

3. The short-bearing approximation yields equations which give simplified relationships among the bearing variables. Eccentricity ratio, attitude angle, location and magnitude of peak film pressure, friction, and required oil flow rate are given as single-line curves when plotted with respect to the capacity number.

4. The capacity number is a basic nondimensional quantity which includes the length-diameter ratio as well as the usual quantities such as load, speed, viscosity, and clearance. These curves are of practical value as charts for analysis of short bearings.

5. The short-bearing approximation and the Sommerfeld equations for long bearings may be considered as similar types of solution based on different assumptions, and each has a range of length-diameter ratios in which it is useful.

Cornell University
Ithaca, N. Y., March 28, 1952

APPENDIX

INTEGRATIONS OF TRIGONOMETRIC FUNCTIONS IN EQUATIONS (14) AND (14a)

For equation (14):

$$\int_0^{\pi} \frac{n \sin\theta \cos\theta \, d\theta}{(1 + n\cos\theta)^3} = \int_0^{\pi} \frac{\cos\theta}{(1 + n\cos\theta)} \times \frac{n \sin\theta \, d\theta}{(1 + n\cos\theta)^2}$$

Substituting:

$$\frac{\cos\theta}{(1 + n\cos\theta)} = \frac{1}{n} - \frac{1}{n(1 + n\cos\theta)}$$

then

$$\int_0^{\pi} \left[\frac{1}{n} - \frac{1}{n(1 + n\cos\theta)}\right] \frac{n \sin\theta \, d\theta}{(1 + n\cos\theta)^2} =$$

$$-\frac{1}{n}\int_0^{\pi} \frac{-n \sin\theta \, d\theta}{(1 + n\cos\theta)^2} + \frac{1}{n}\int_0^{\pi} \frac{-n \sin\theta \, d\theta}{(1 + n\cos\theta)^3} =$$

$$\left[\frac{1}{n(1 + n\cos\theta)}\right]_0^{\pi} - \left[\frac{1}{2n(1 + n\cos\theta)^2}\right]_0^{\pi} =$$

$$\frac{1}{n}\left[\frac{1}{(1 - n)} - \frac{1}{(1 + n)}\right] - \frac{1}{2n}\left[\frac{1}{(1 - n)^2} - \frac{1}{(1 + n)^2}\right] =$$

$$-\frac{2n^2}{(1 - n^2)^2}$$

For equation (14a):

$$\int_0^{\pi} \frac{n \sin^2\theta \, d\theta}{(1 + n \cos \theta)^3} = - \int_0^{\pi} \sin \theta \times \frac{-n \sin \theta \, d\theta}{(1 + n \cos \theta)^3}$$

By using

$$u = \sin \theta$$

$$du = \cos \theta \, d\theta$$

$$dv = \frac{-n \sin \theta \, d\theta}{(1 + n \cos \theta)^3}$$

$$v = - \frac{1}{2(1 + n \cos \theta)^2}$$

and if

$$\left[\frac{\sin \theta}{2(1 + n \cos \theta)^2} \right]_0^{\pi} = 0$$

then

$$\left[\frac{\sin \theta}{2(1 + n \cos \theta)^2} \right]_0^{\pi} - \frac{1}{2} \int_0^{\pi} \frac{\cos \theta \, d\theta}{(1 + n \cos \theta)^2} = - \frac{1}{2} \int_0^{\pi} \frac{\cos \theta \, d\theta}{(1 + n \cos \theta)^2} =$$

$$- \frac{1}{2} \int_0^{\pi} \left[\frac{1}{n} - \frac{1}{n(1 + n \cos \theta)} \right] \frac{d\theta}{(1 + n \cos \theta)} =$$

$$- \frac{1}{2n} \int_0^{\pi} \frac{d\theta}{(1 + n \cos \theta)} + \frac{1}{2n} \int_0^{\pi} \frac{d\theta}{(1 + n \cos \theta)^2}$$

Using Sommerfeld's substitutions:

$$d\theta = \frac{(1 - n^2)^{1/2}}{(1 - n \cos \alpha)} d\alpha$$

and

$$1 + n \cos \theta = \frac{1 - n^2}{(1 - n \cos \alpha)}$$

then

$$-\frac{1}{2n}\int_0^{\pi} \frac{(1 - n^2)^{1/2} d\alpha}{(1 - n \cos \alpha)} \times \frac{(1 - n \cos \alpha)}{(1 - n^2)} + \frac{1}{2n}\int_0^{\pi} \frac{(1 - n^2)^{1/2} d\alpha}{(1 - n \cos \alpha)} \times \frac{(1 - n \cos \alpha)^2}{(1 - n^2)^2} =$$

$$-\frac{1}{2n(1 - n^2)^{1/2}}\int_0^{\pi} d\alpha + \frac{1}{2n(1 - n^2)^{3/2}}\int_0^{\pi} (1 - n \cos \alpha)\, d\alpha =$$

$$-\frac{\alpha}{2n(1 - n^2)^{1/2}}\Bigg]_0^{\pi} + \frac{1}{2n(1 - n^2)^{3/2}}\Big[\alpha - n \sin \alpha\Big]_0^{\pi} =$$

$$-\frac{\pi}{2n(1 - n^2)^{1/2}} + \frac{\pi}{2n(1 - n^2)^{3/2}} =$$

$$\frac{\pi n}{2(1 - n^2)^{3/2}}$$

REFERENCES

1. Reynolds, O.: On the Theory of Lubrication and Its Application to Mr. Beauchamp Tower's Experiments, Including an Experimental Determination of the Viscosity of Olive Oil. Phil. Trans. Roy. Soc. (London), ser. A, vol. 177, 1886, pp. 157-234.

2. Michell, A. G. M.: The Lubrication of Plane Surfaces. Zeit. Math. und Phys., vol. 52, 1905, pp. 123-137.

3. Kingsbury, Albert: Problems in Theory of Fluid-Film Lubrication, with Experimental Method of Solution. Trans. A.S.M.E., APM-53-5, vol. 53, 1931, pp. 59-74.

4. Christopherson, D. G.: A New Mathematical Method for the Solution of Film Lubrication Problems. Proc. Institution Mech. Eng. (London), vol. 146, no. 3, 1941, pp. 126-135.

5. Cameron, A., and Wood, W. L.: The Full Journal Bearing. Proc. Institution Mech. Eng. (London), vol. 161, W.E.P. Nos. 47-54, 1949, pp. 59-72.

6. Navier, Claude L. M. H.: Memoir on the Laws of Fluid Motion. Mém., acad. sci. (Paris), vol. 6, 1827, p. 389.

7. Stokes, G. G.: On the Theories of the Internal Friction of Fluids in Motion. Trans. Cambridge Phil. Soc., vol. 8, 1845.

8. Sommerfeld, A.: The Hydrodynamic Theory of Lubrication Friction. Zeit. Math. und Phys., vol. 50, nos. 1 and 2, 1904, pp. 97-155.

9. Harrison, W. J.: The Hydrodynamic Theory of Lubrication with Special Reference to Air as a Lubricant. Proc. Cambridge Phil. Soc., vol. 22, no. 3, 1913, pp. 39-54.

10. Michell, A. G. M.: Progress in Fluid-Film Lubrication. Trans. A.S.M.E., MSP-51-21, vol. 51, 1929, pp. 153-163.

11. Cardullo, F. E.: Some Practical Deductions from Theory of Lubrication of Short Cylindrical Bearings. Trans. A.S.M.E., MSP-52-12, vol. 52, 1930, pp. 143-153.

12. McKee, S. A., and McKee, T. R.: Pressure Distribution in Oil Films of Journal Bearings. Trans. A.S.M.E., RP-54-8, vol. 54, 1932, pp. 149-165.

13. Bradford, L. J., and Grunder, L. J.: Oil Film Pressures in a Complete Journal Bearing. Eng. Exp. Station Bull. No. 39, Penn. State College Bull., vol. XXIV, no. 40, Sept. 8, 1930, pp. 1-50.

14. DuBois, G. B., Mabie, H. H., and Ocvirk, F. W.: Experimental Investigation of Oil Film Pressure Distribution for Misalined Plain Bearings. NACA TN 2507, 1951.

15. DuBois, G. B., and Ocvirk, F. W.: Experimental Investigation of Eccentricity Ratio, Friction, and Oil Flow of Short Journal Bearings. NACA TN 2809, 1952.

16. Bradford, L. J., and Davenport, C. C.: Characteristic Curves for Fluid Film Lubricated Journal Bearings. Refrigerating Eng., vol. 24, Dec. 1932, pp. 343-347.

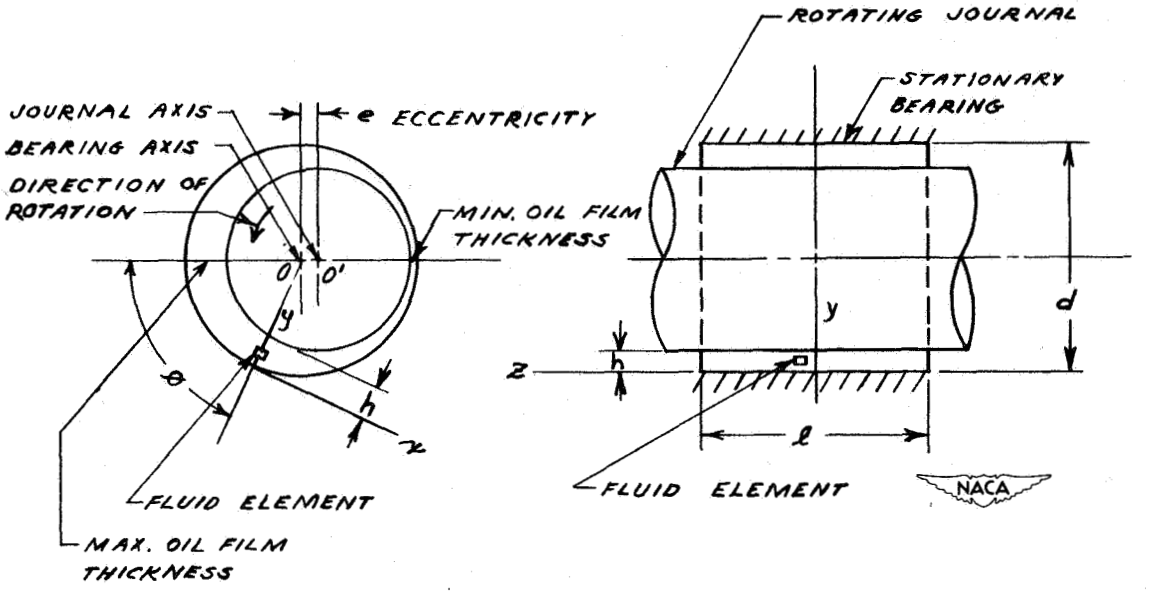

Figure 1.- Fluid element in converging oil film of cylindrical bearing with endwise flow.

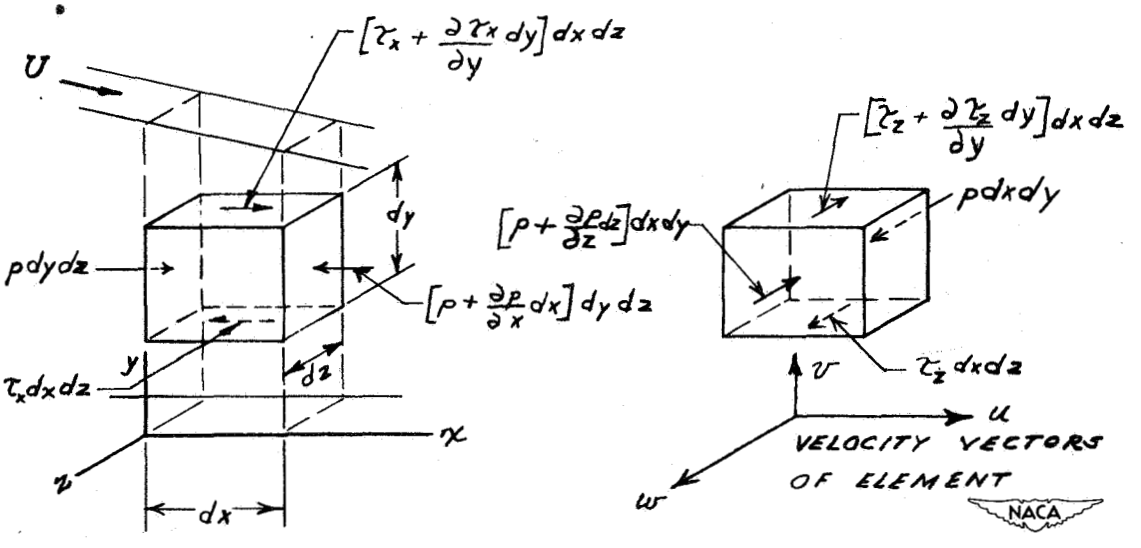

(a) In x-direction where $\frac{\partial \tau_x}{\partial y} = \frac{\partial p}{\partial x}$.

(b) In z-direction where $\frac{\partial \tau_z}{\partial y} = \frac{\partial p}{\partial z}$.

Figure 2.- Assumed forces acting on fluid element.

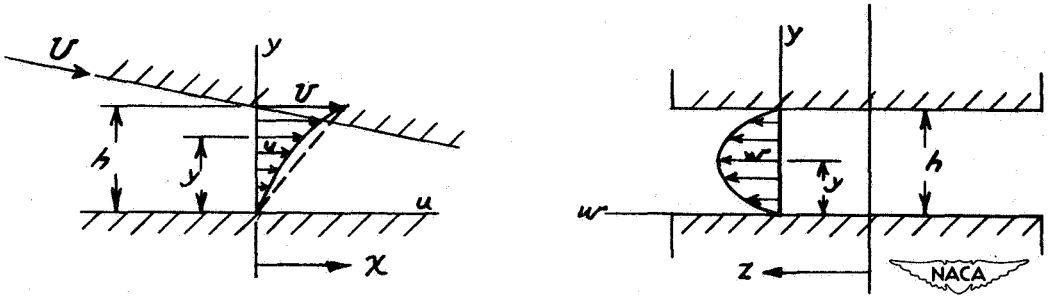

(a) In x-direction where
$$u = \frac{Uy}{h} + \frac{1}{2\mu}\frac{\partial p}{\partial x}y(y - h).$$

(b) In z-direction where
$$w = \frac{1}{2\mu}\frac{\partial p}{\partial z}y(y - h).$$

Figure 3.- Velocity profiles in oil film.

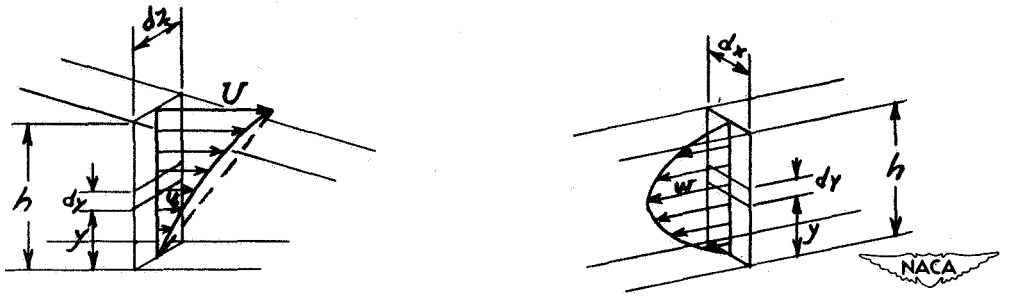

(a) Normal to x-direction where
$$q_x = \left(\frac{Uh}{2} - \frac{h^3}{12\mu}\frac{\partial p}{\partial x}\right)dz.$$

(b) Normal to z-direction where
$$q_z = \left(\frac{-h^3}{12\mu}\frac{\partial p}{\partial z}\right)dx.$$

Figure 4.- Quantity of flow per unit time through elemental plane.

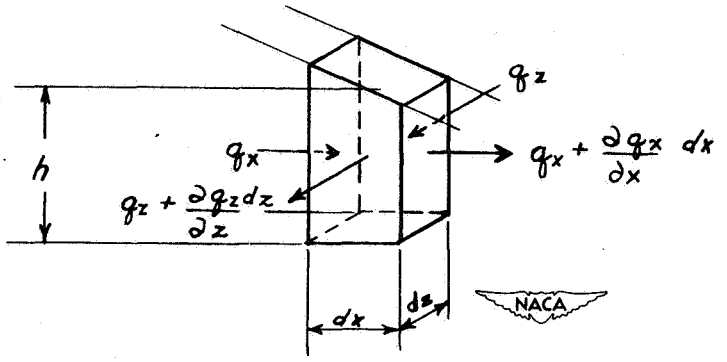

Figure 5.- Quantities of flow entering and leaving fluid element as given by $\frac{\partial q_x}{\partial x} dx + \frac{\partial q_z}{\partial z} dz = 0$.

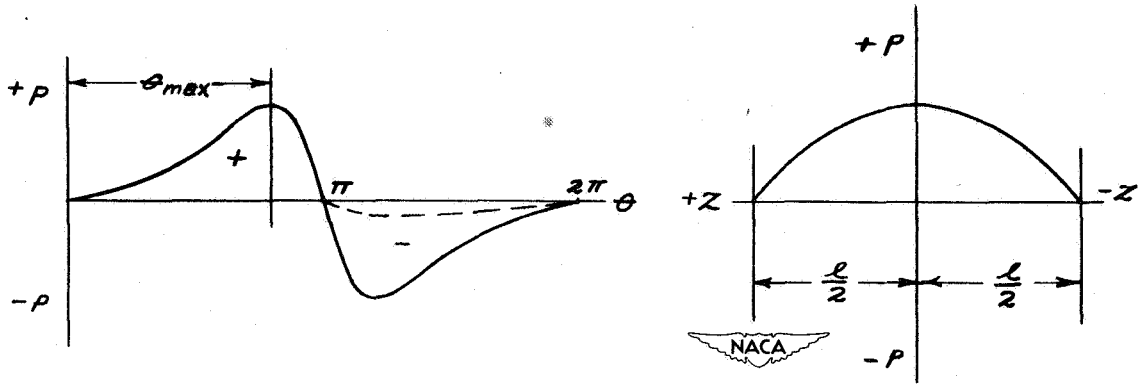

(a) In x-direction (b) In z-direction

Figure 6.- Pressure distribution in a full cylindrical bearing as given by $p = \frac{3\mu U}{rc_r^2}\left(\frac{l^2}{4} - z^2\right)\frac{n \sin \theta}{(1 + n \cos \theta)^3}$.

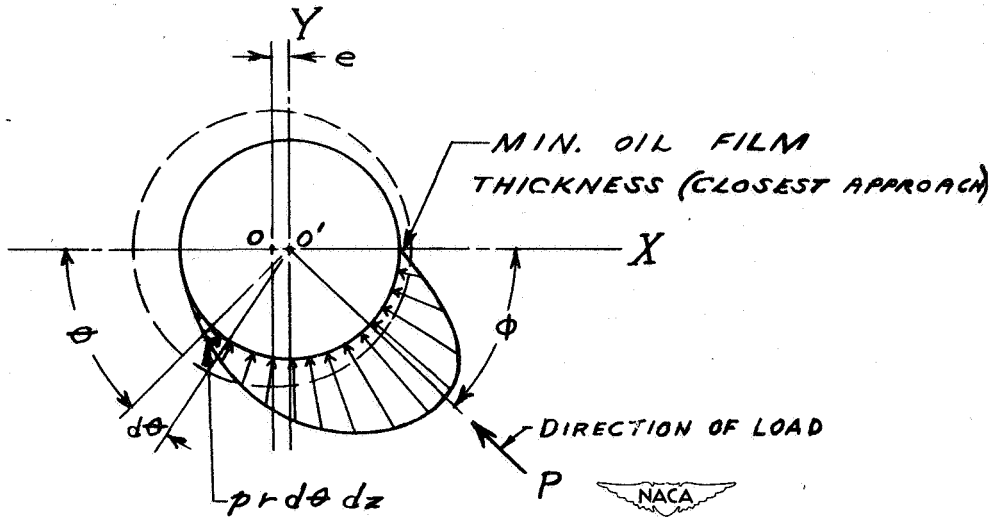

Figure 7.- System of coordinates chosen for integration of pressures and determination of attitude angle ϕ.

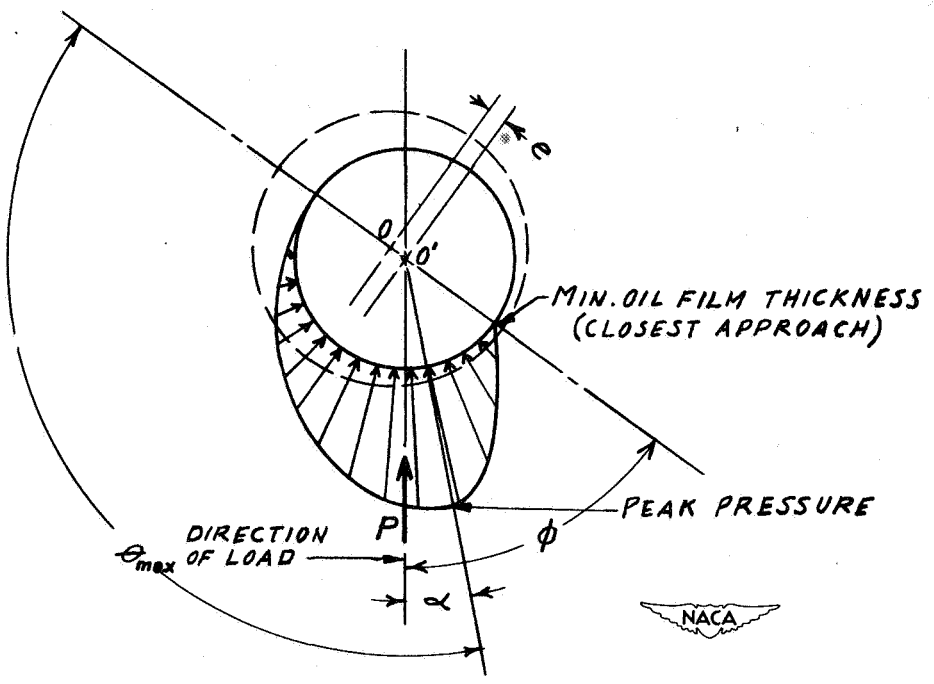

Figure 8.- Diagram showing attitude angle ϕ, maximum-pressure angle θ_{max}, and peak-pressure angle α.

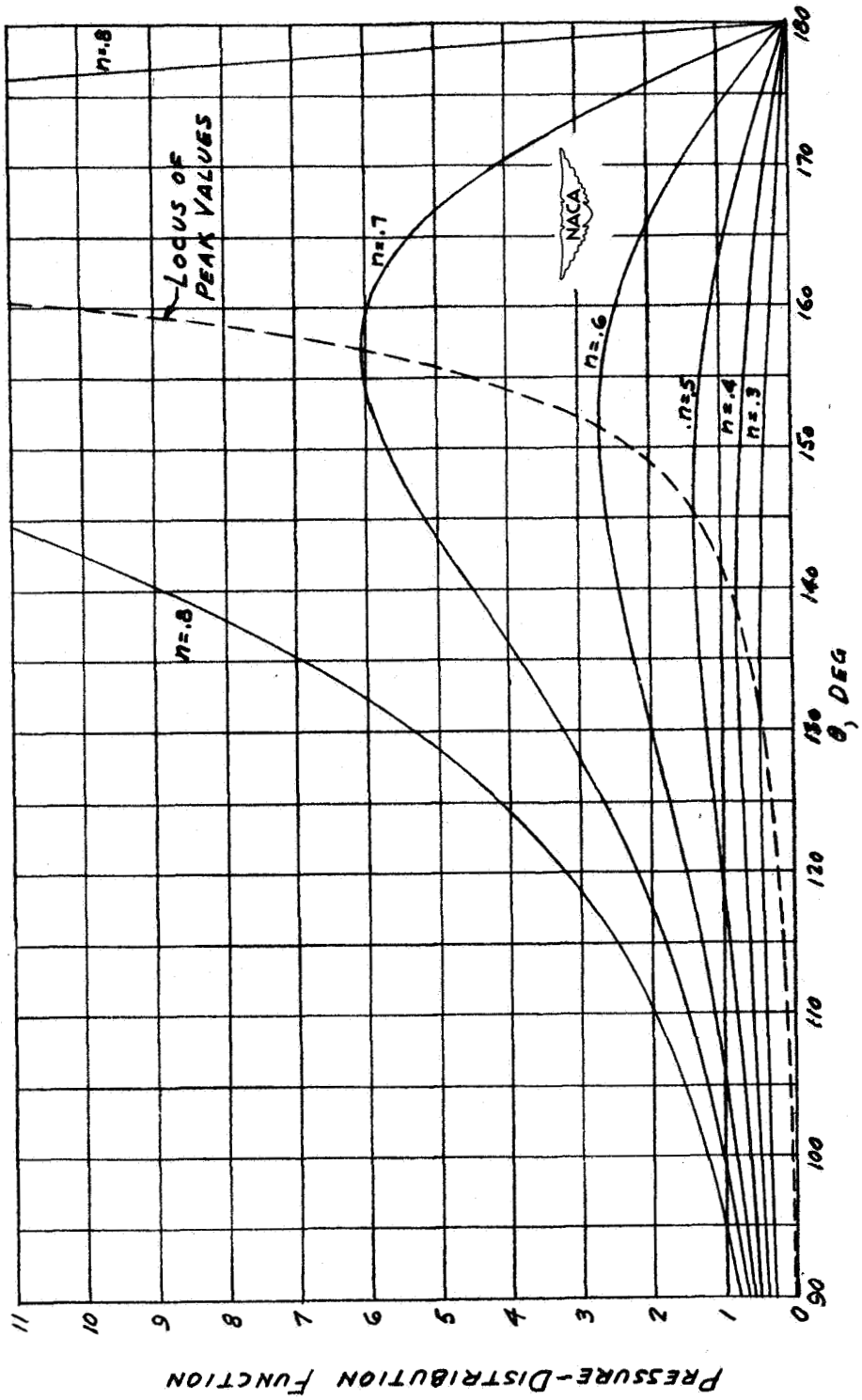

Figure 9.- Circumferential pressure distribution in short journal bearings as given by distribution function $\frac{n \sin \theta}{(1 + n \cos \theta)^3}$ of equation (13).

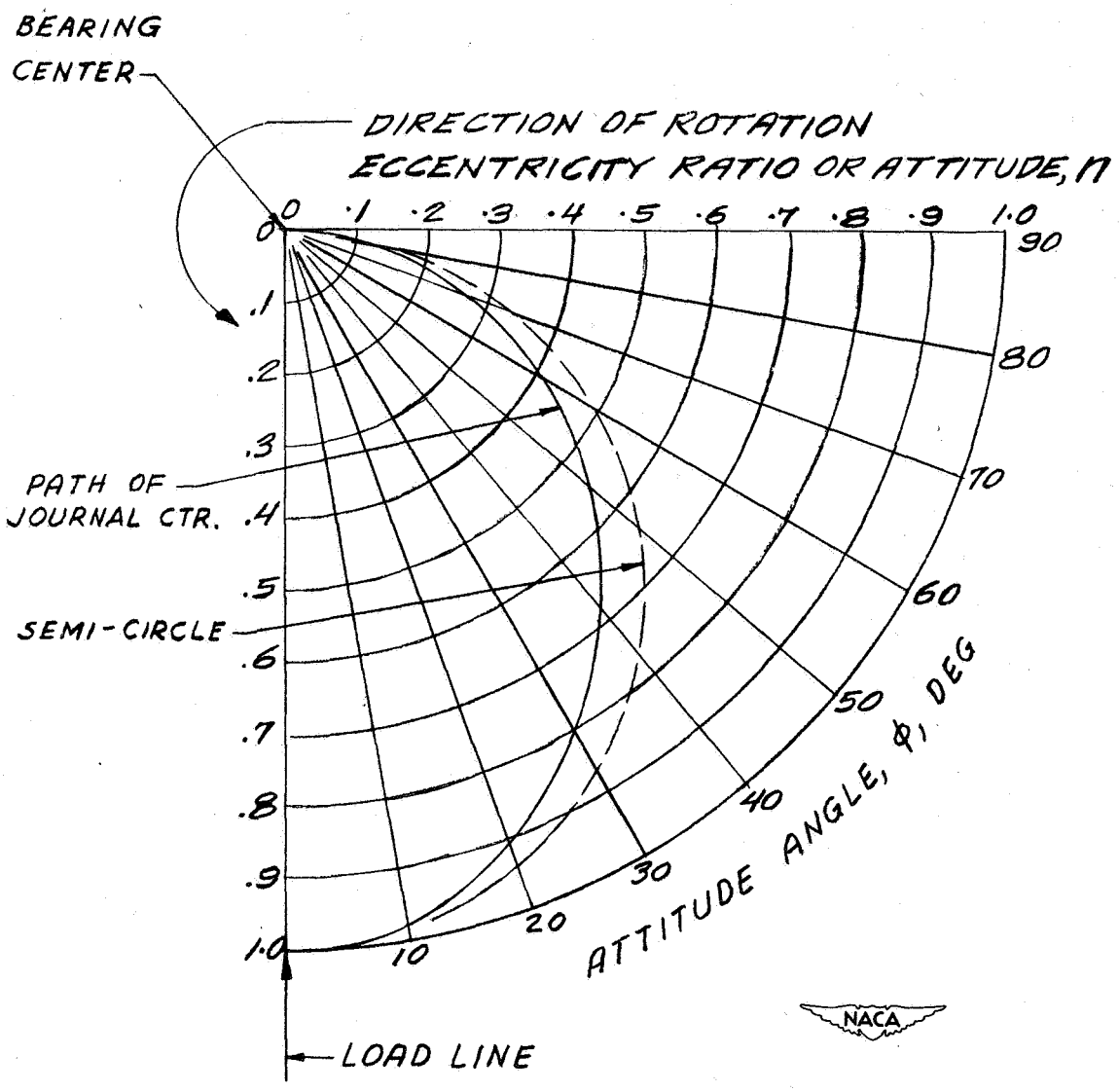

Figure 10.- Plot of eccentricity ratio against attitude angle of short bearings showing position of journal center with respect to bearing center (based on equation (18)).

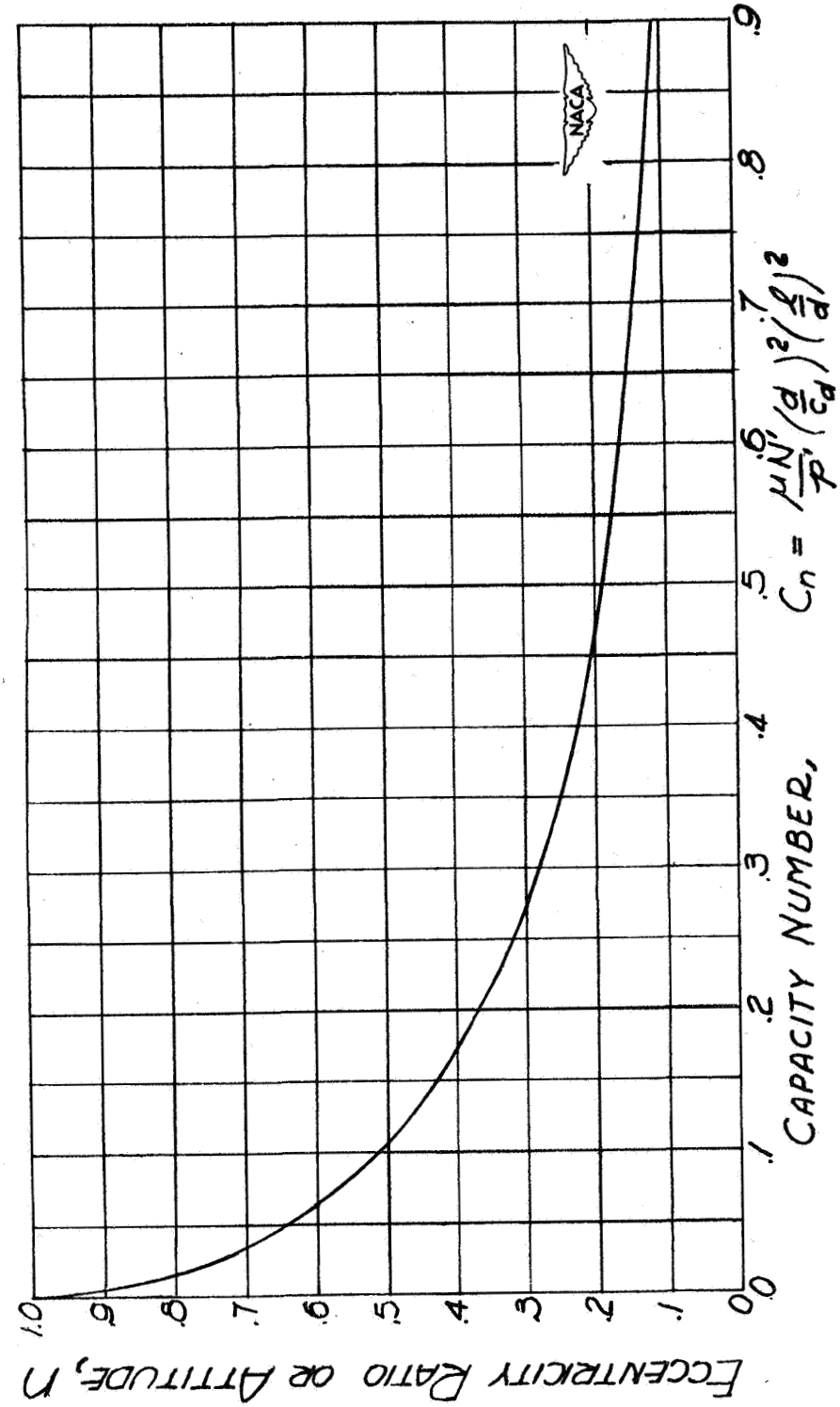

Figure 11.- Plot of eccentricity ratio against capacity number for short journal bearings (based on equation (17)).

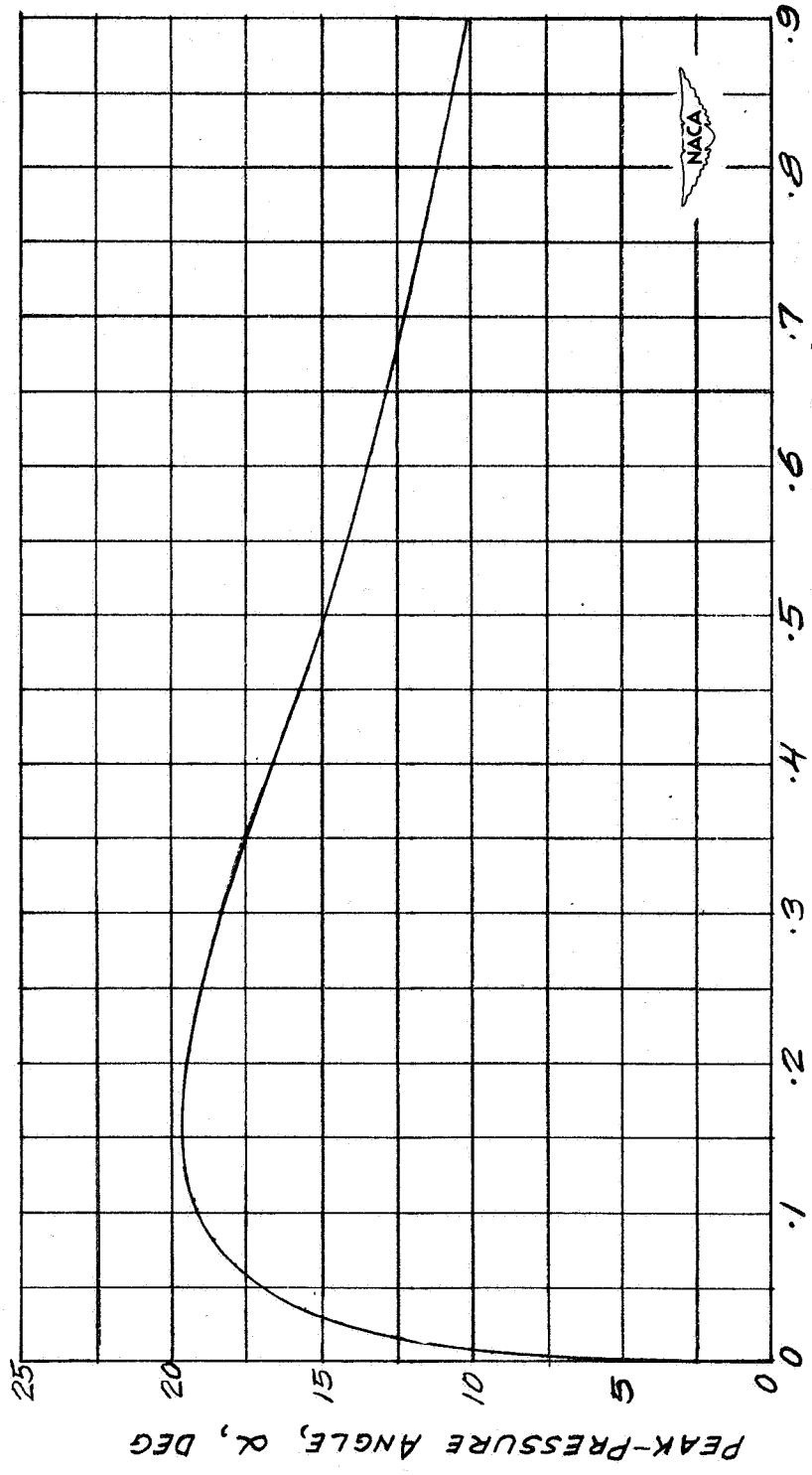

Figure 12.- Plot of peak-pressure angle against capacity number for short journal bearings (based on equations (18), (19), and (20)).

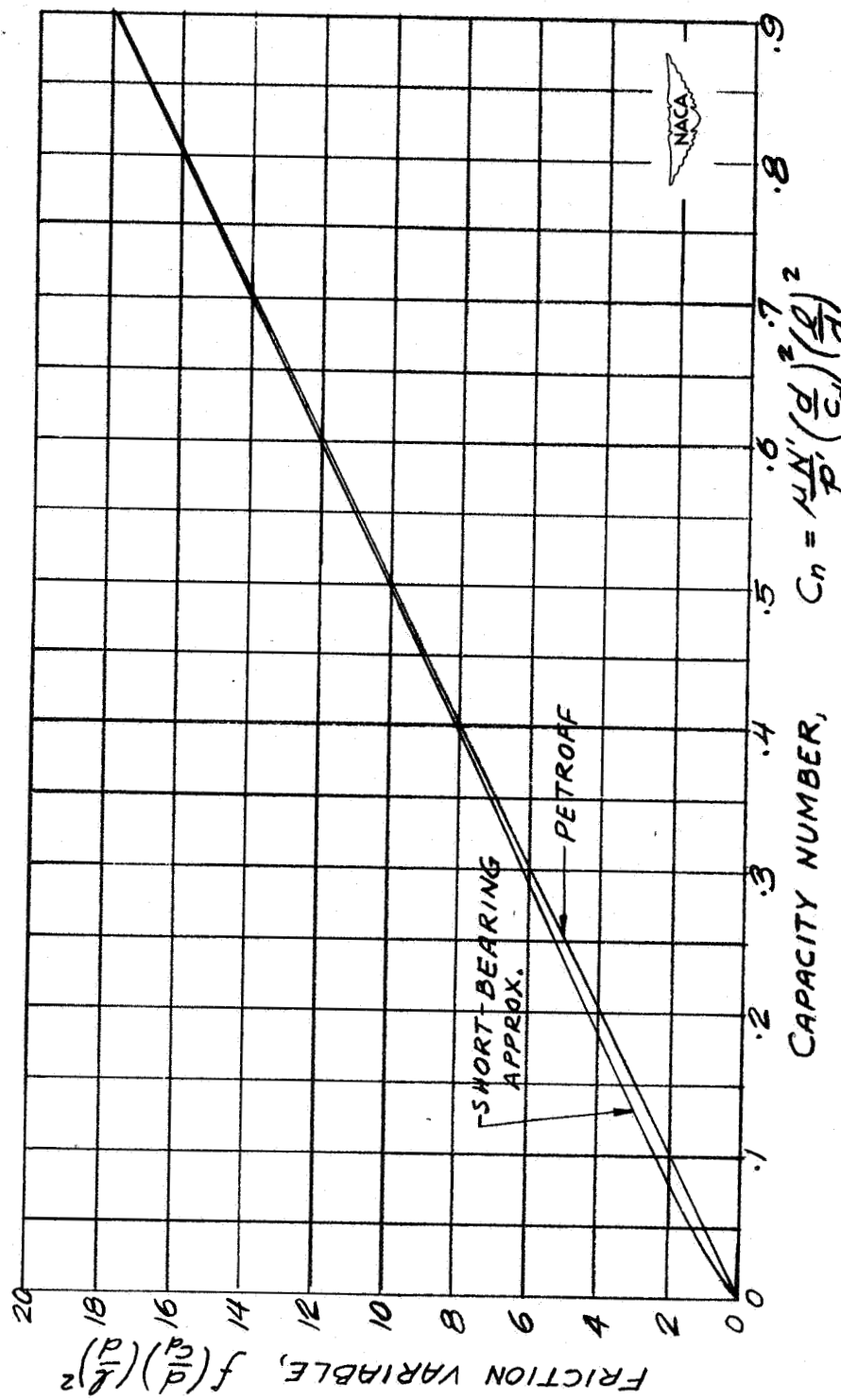

Figure 13.- Plot of friction variable against capacity number for short journal bearings (based on equation (21)).

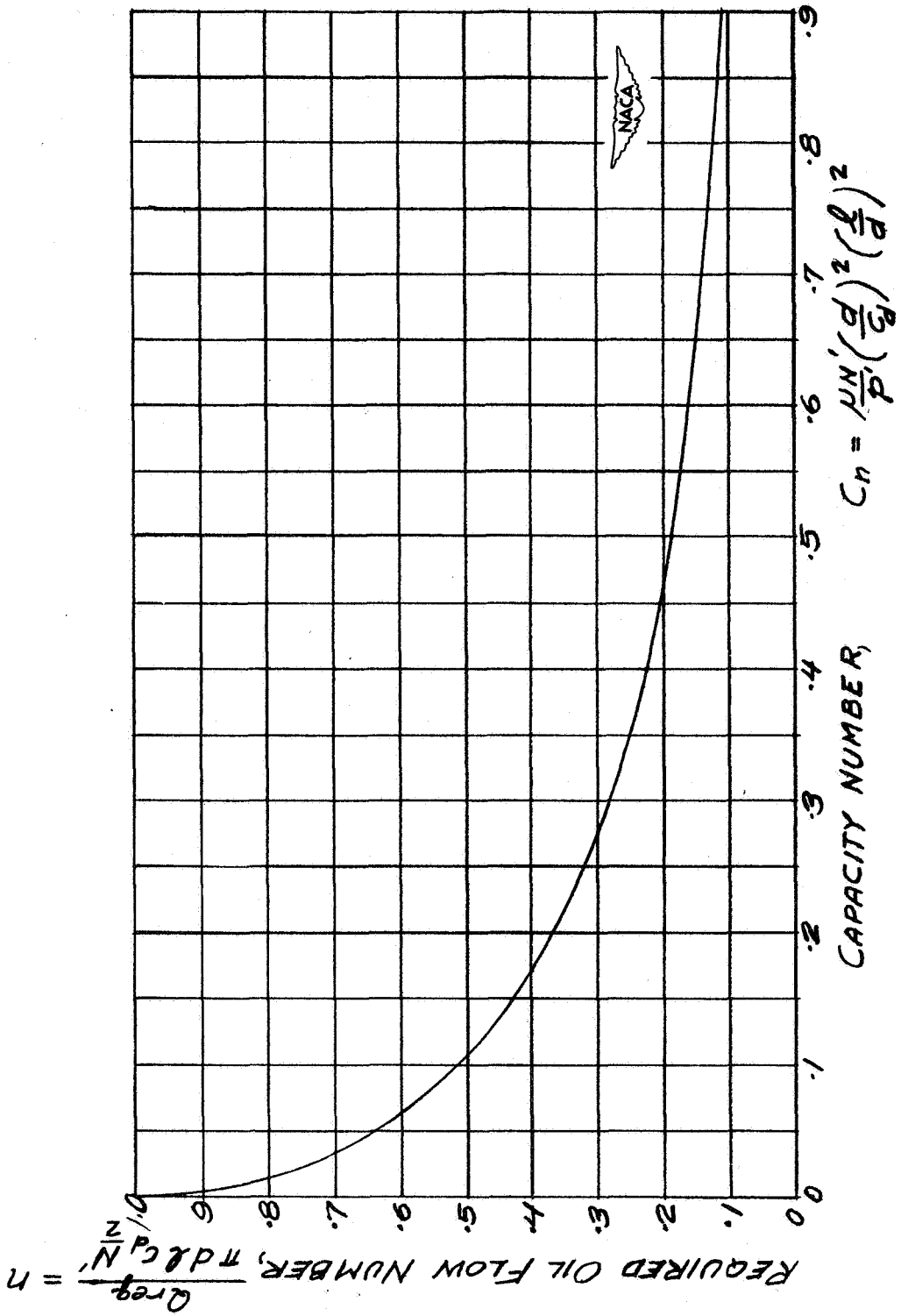

Figure 14.- Plot of required oil flow number against capacity number for short journal bearings (based on equations (17) and (23)).

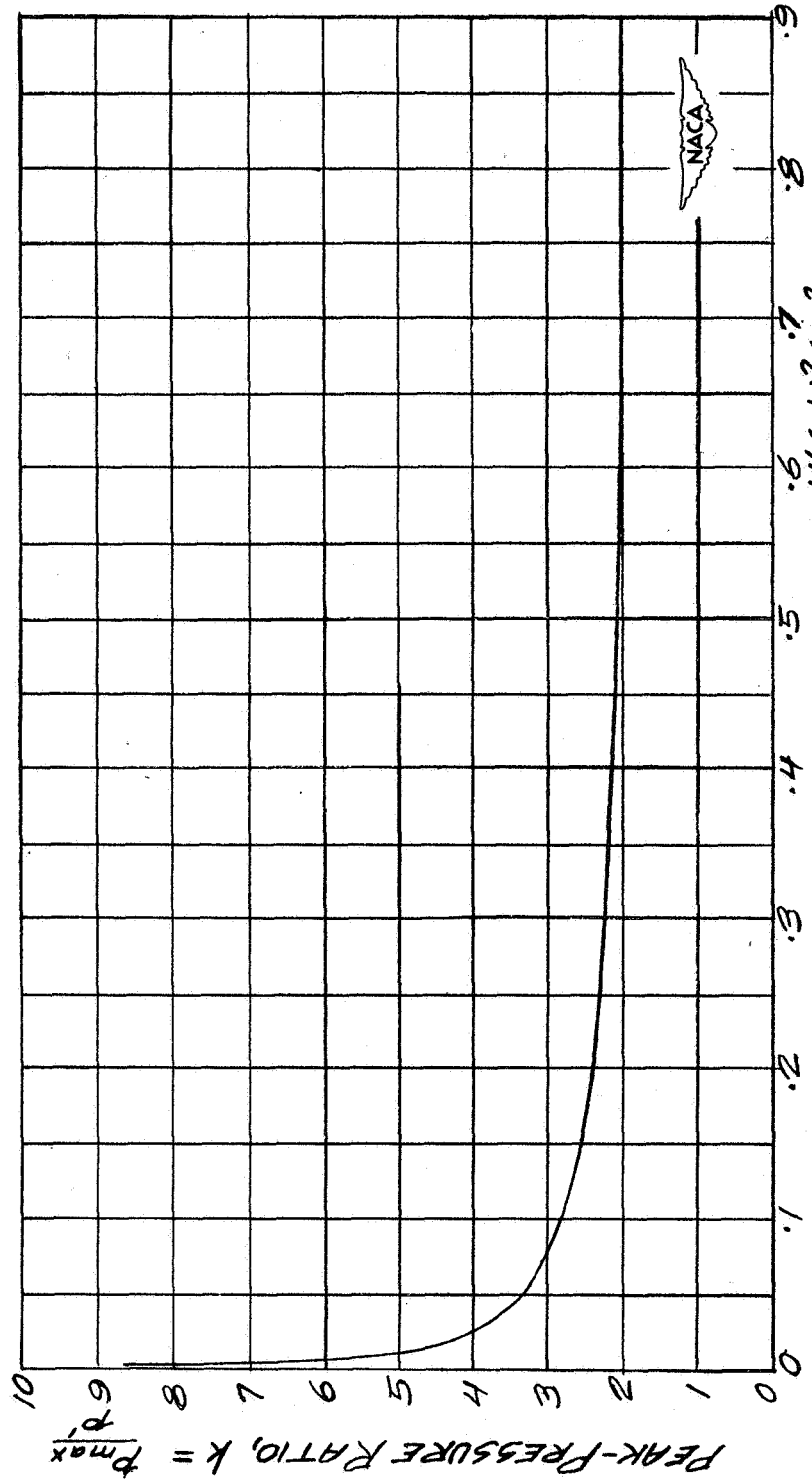

Figure 15.- Plot of peak-pressure ratio against capacity number for short journal bearings (based on equation (24)).

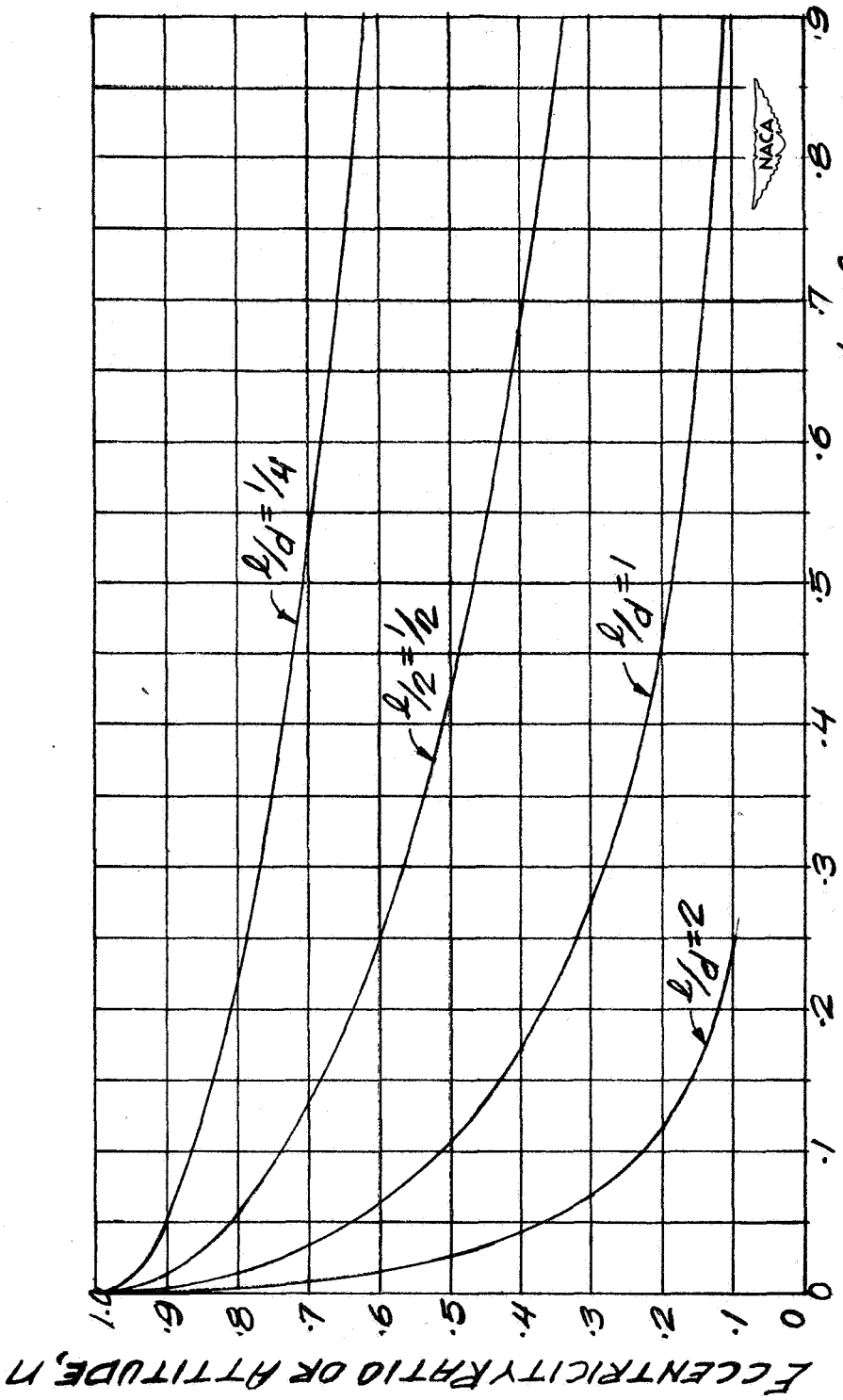

Figure 16.- Plot of eccentricity ratio against Sommerfeld number for short journal bearings (based on equation (17)).

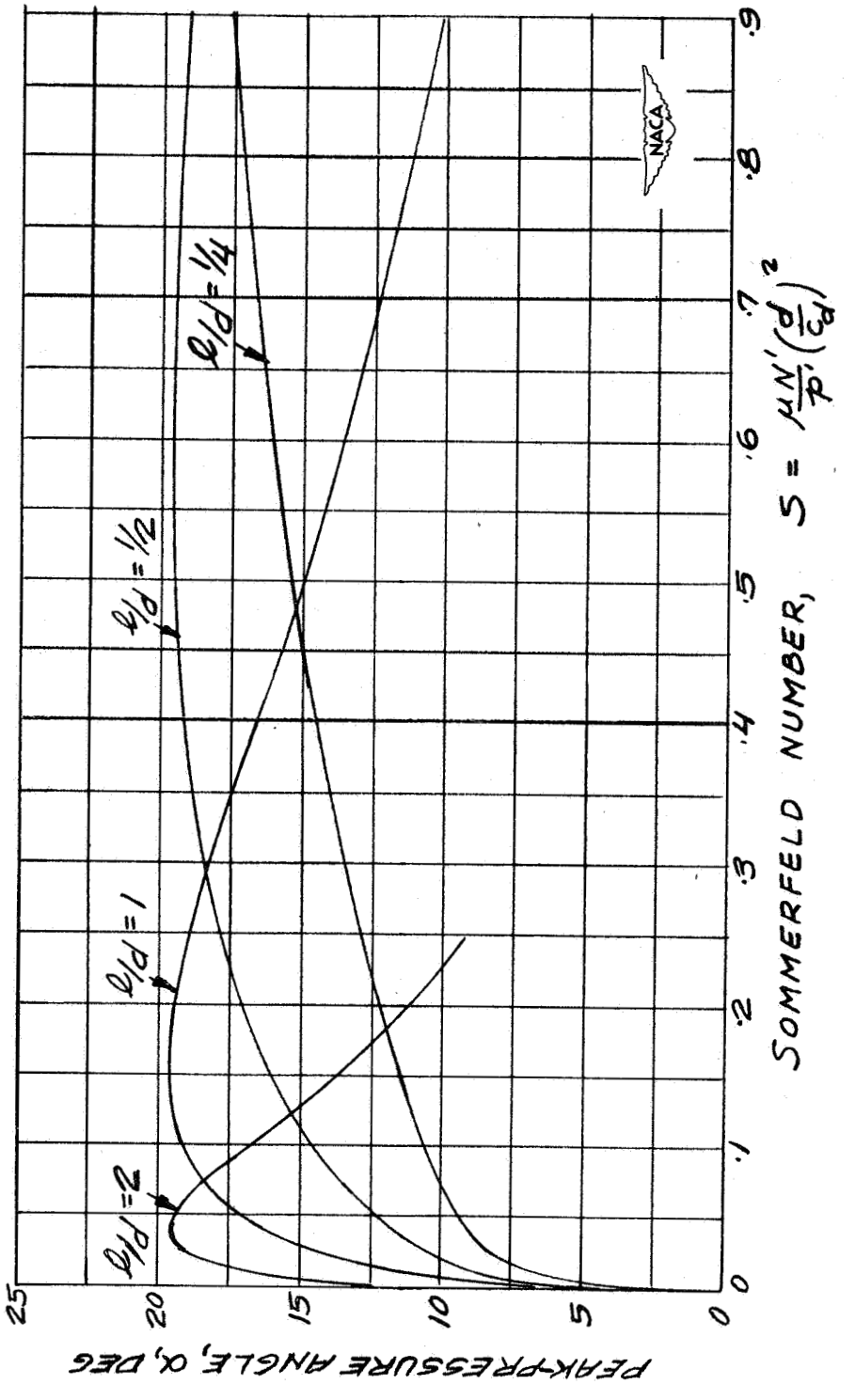

Figure 17.- Plot of peak-pressure angle against Sommerfeld number for short journal bearings (based on equations (18), (19), and (20)).

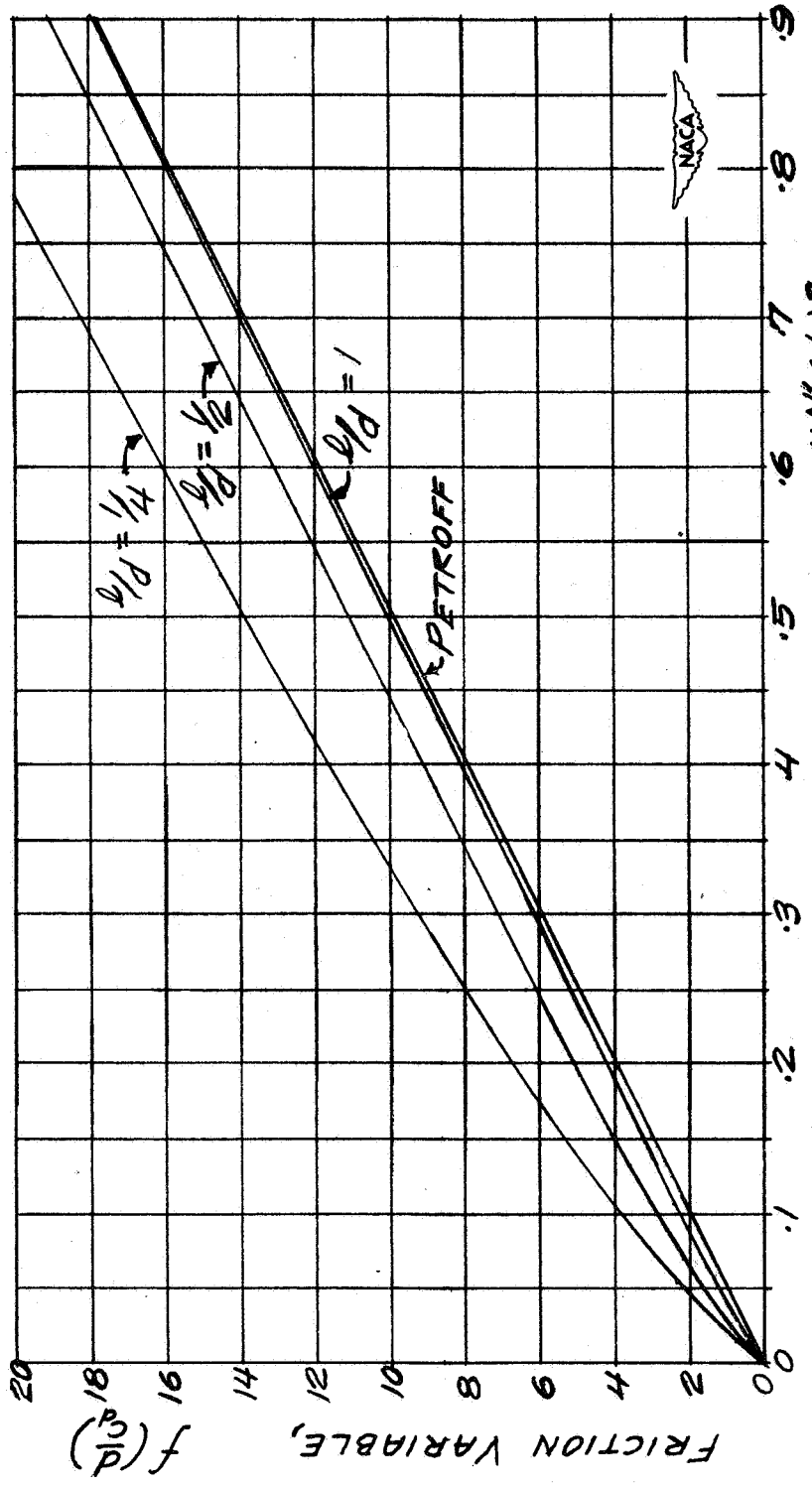

Figure 18.- Plot of friction variable against Sommerfeld number for short journal bearings (based on equation (21)).

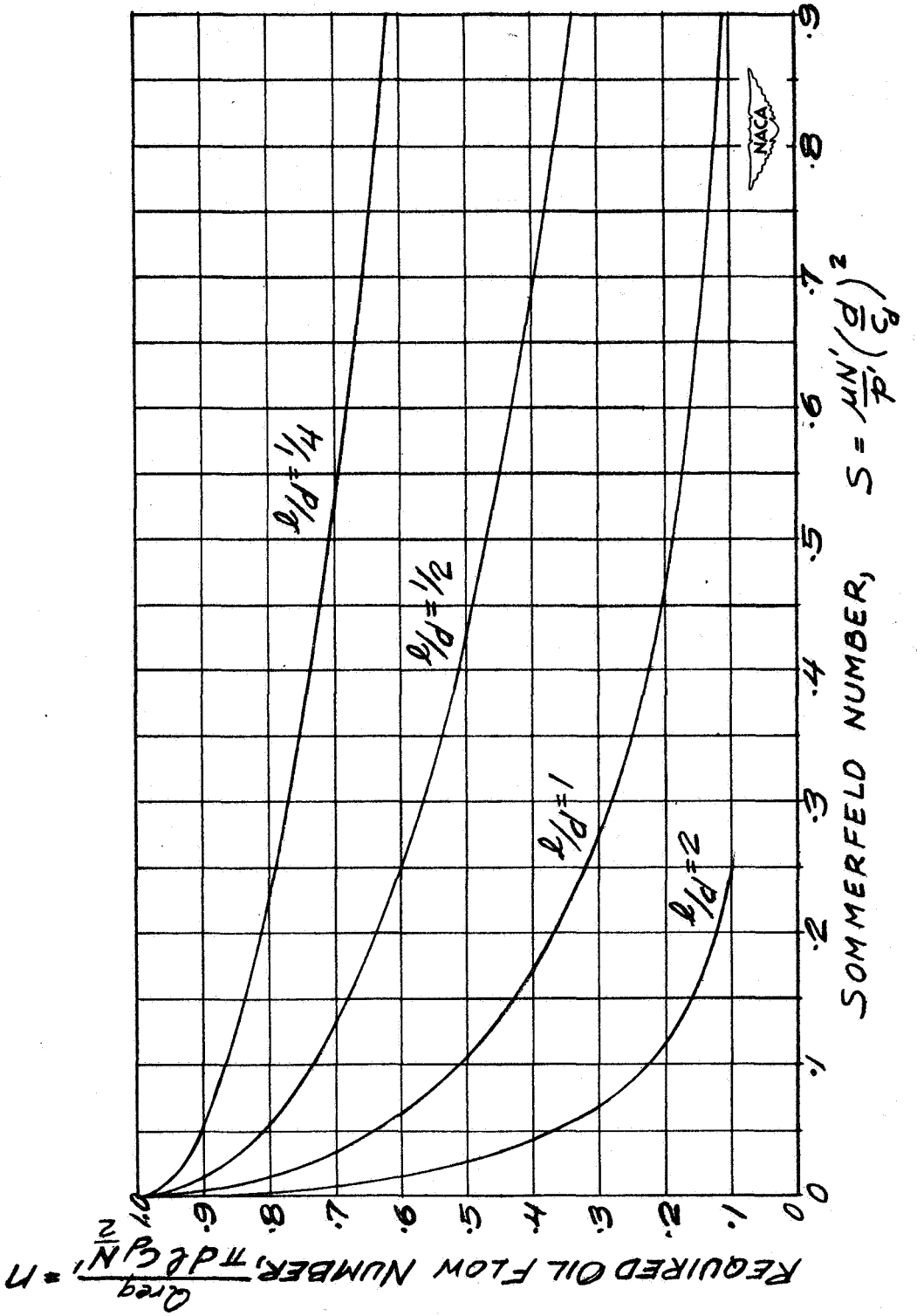

Figure 19.- Plot of required oil flow number against Sommerfeld number for short journal bearings (based on equations (17) and (23)).

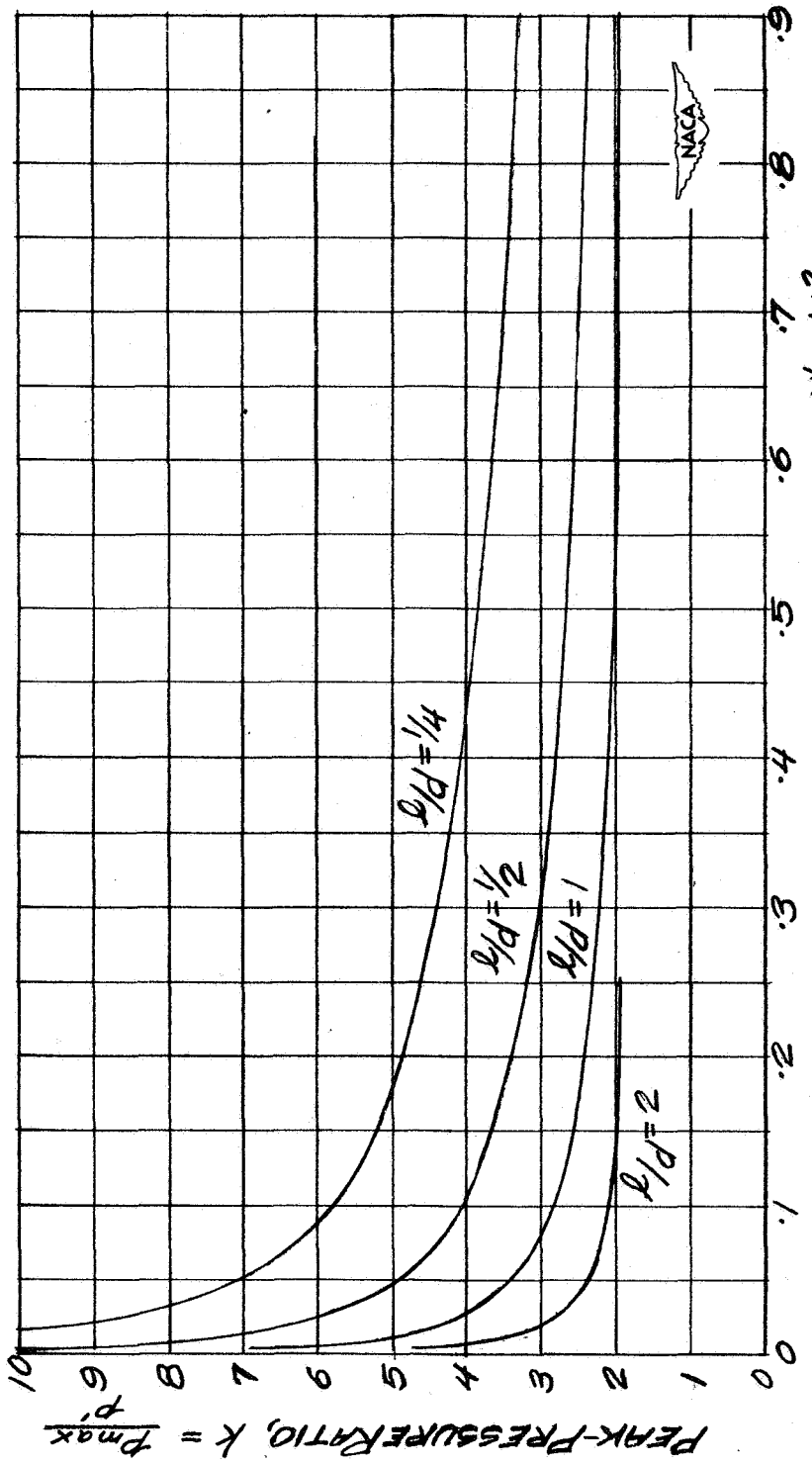

Figure 20.- Plot of peak-pressure ratio against Sommerfeld number for short journal bearings (based on equation (24)).

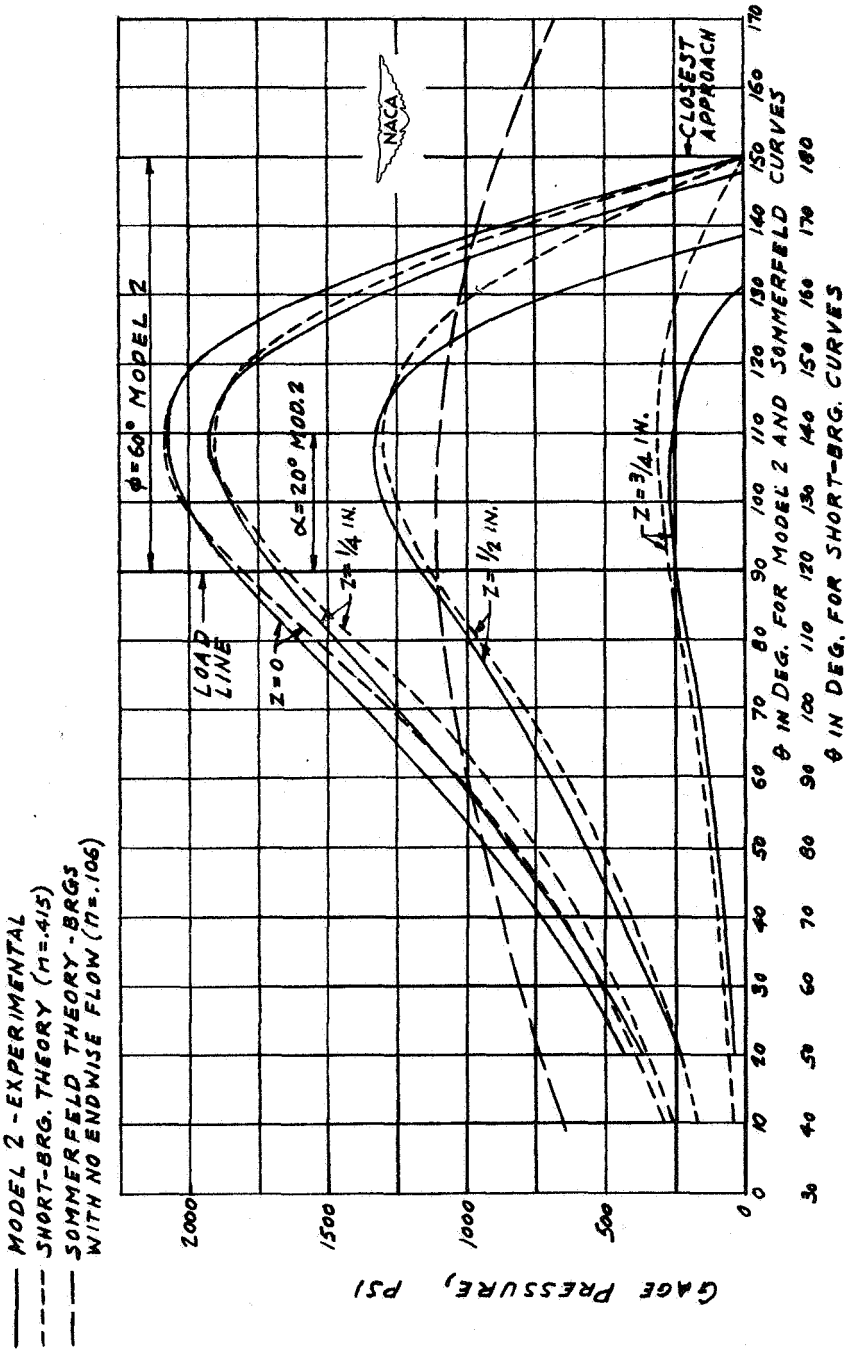

Figure 21.- Comparison of theoretical pressure distribution with experimental pressure distribution of model 2 of reference 14. Load, 2200 pounds; speed, 5000 rpm; average temperature, 197° F; viscosity, 2.42 × 10^{-6} reyns; bearing length, $1\frac{5}{8}$ inches; bearing diameter, $1\frac{5}{8}$ inches; radial clearance at 197° F, 0.001 inch.

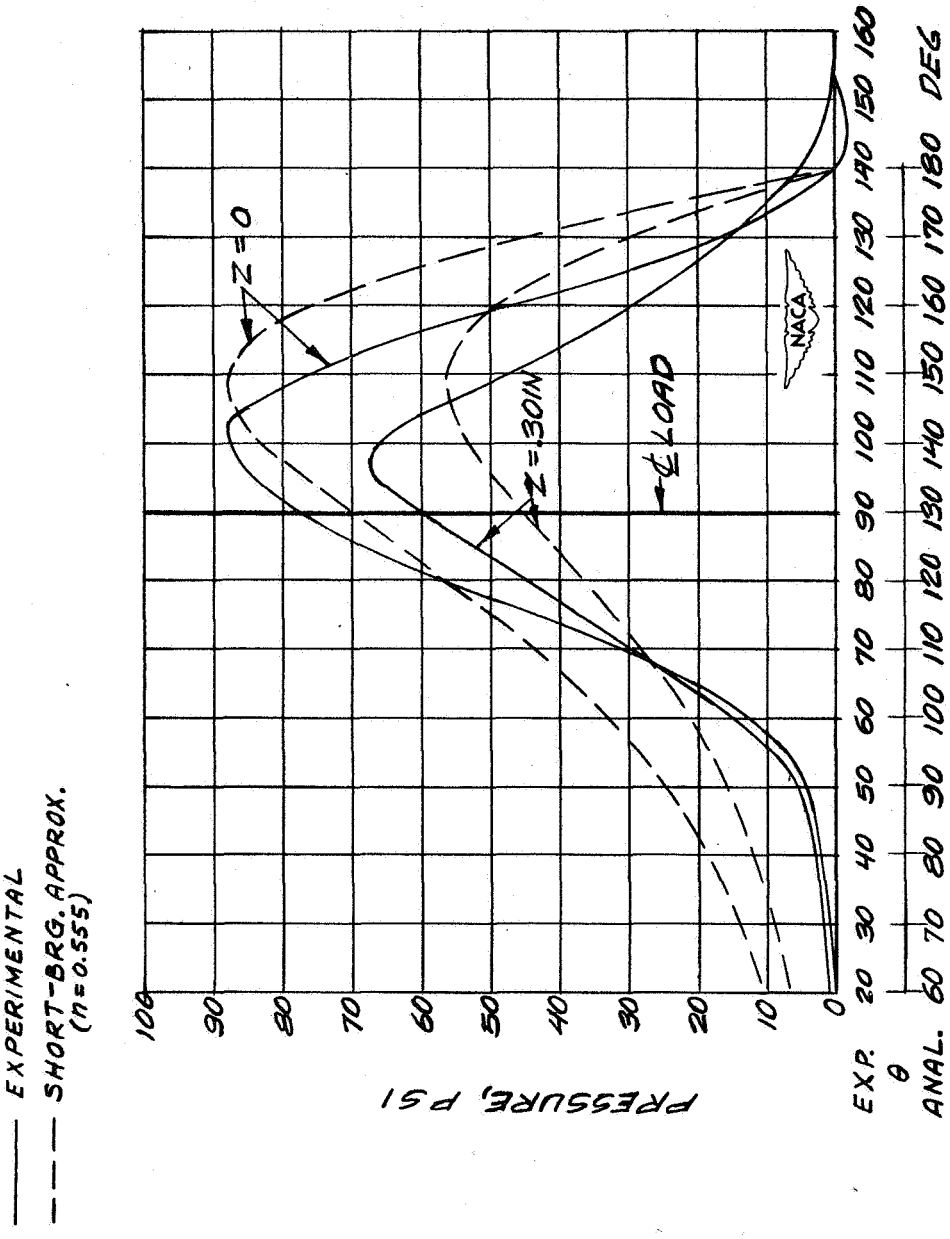

Figure 22.- Comparison of analytical pressure distribution with experimental pressure distribution from test no. 1 by McKee and McKee (reference 12). Load, 25 pounds; speed, 565 rpm; viscosity, 42.9 centipoises; bearing length, 1.0 inch; bearing diameter, 0.8703 inch; radial clearance, 0.0025 inch.

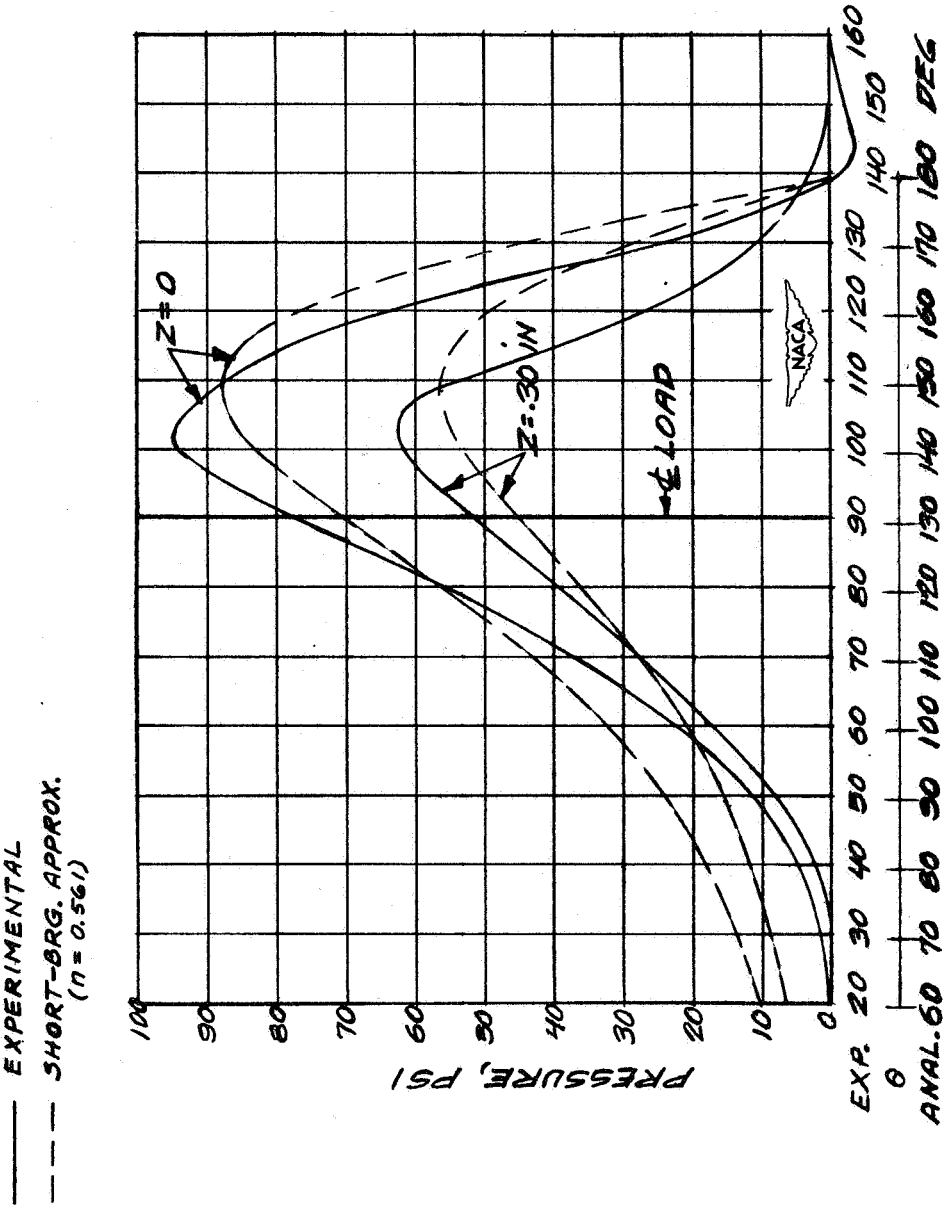

Figure 23.- Comparison of analytical pressure distribution with experimental pressure distribution from test no. 2 by McKee and McKee (reference 12). Load, 25 pounds; speed, 592 rpm; viscosity, 39.4 centipoises; bearing length, 1.0 inch; bearing diameter, 0.8703 inch; radial clearance, 0.0025 inch.

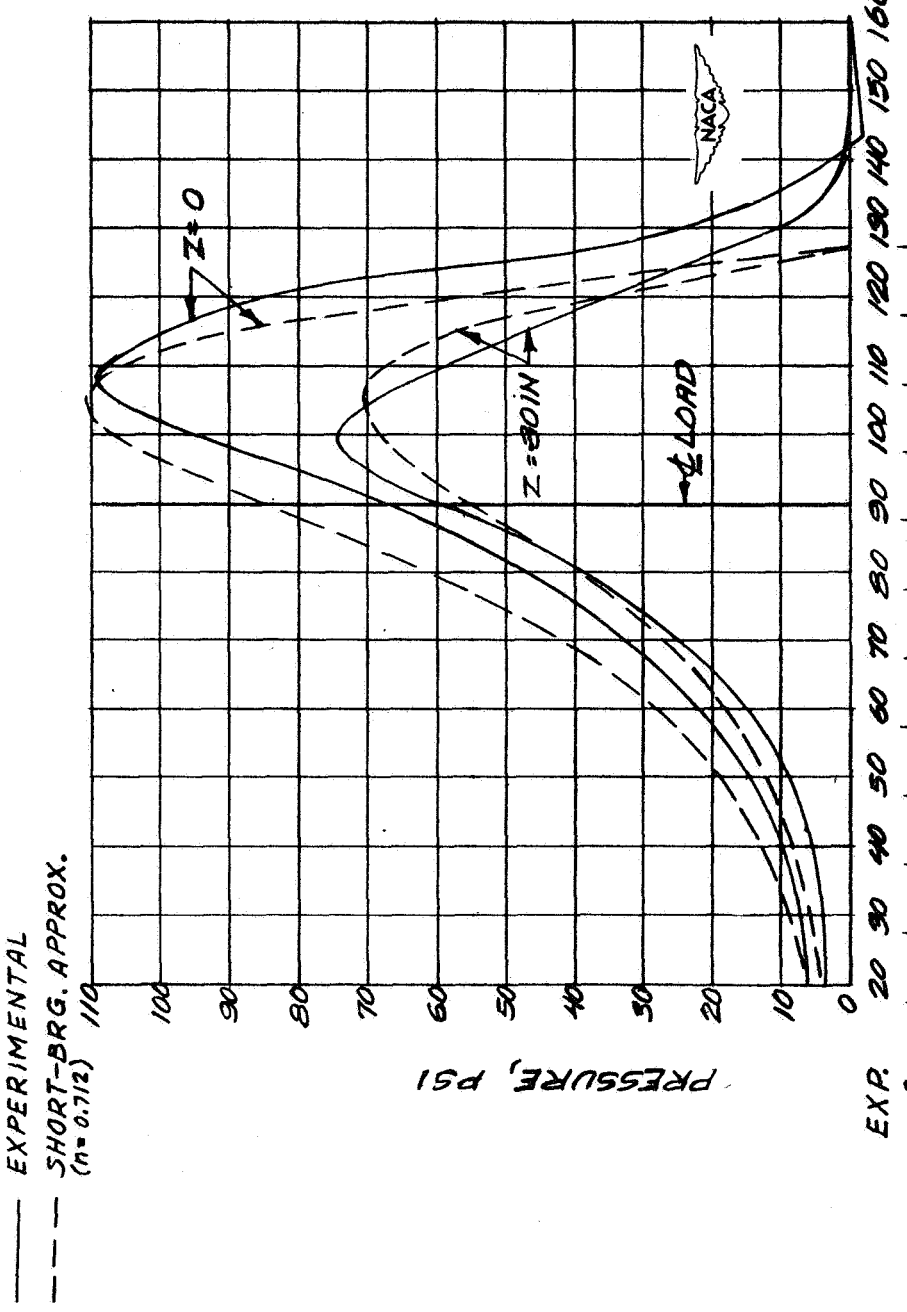

Figure 24.- Comparison of analytical pressure distribution with experimental pressure distribution from test no. 3 by McKee and McKee (reference 12). Load, 25 pounds; speed, 244 rpm; viscosity, 36.5 centipoises; bearing length, 1.0 inch; bearing diameter, 0.8703 inch; radial clearance, 0.0025 inch.

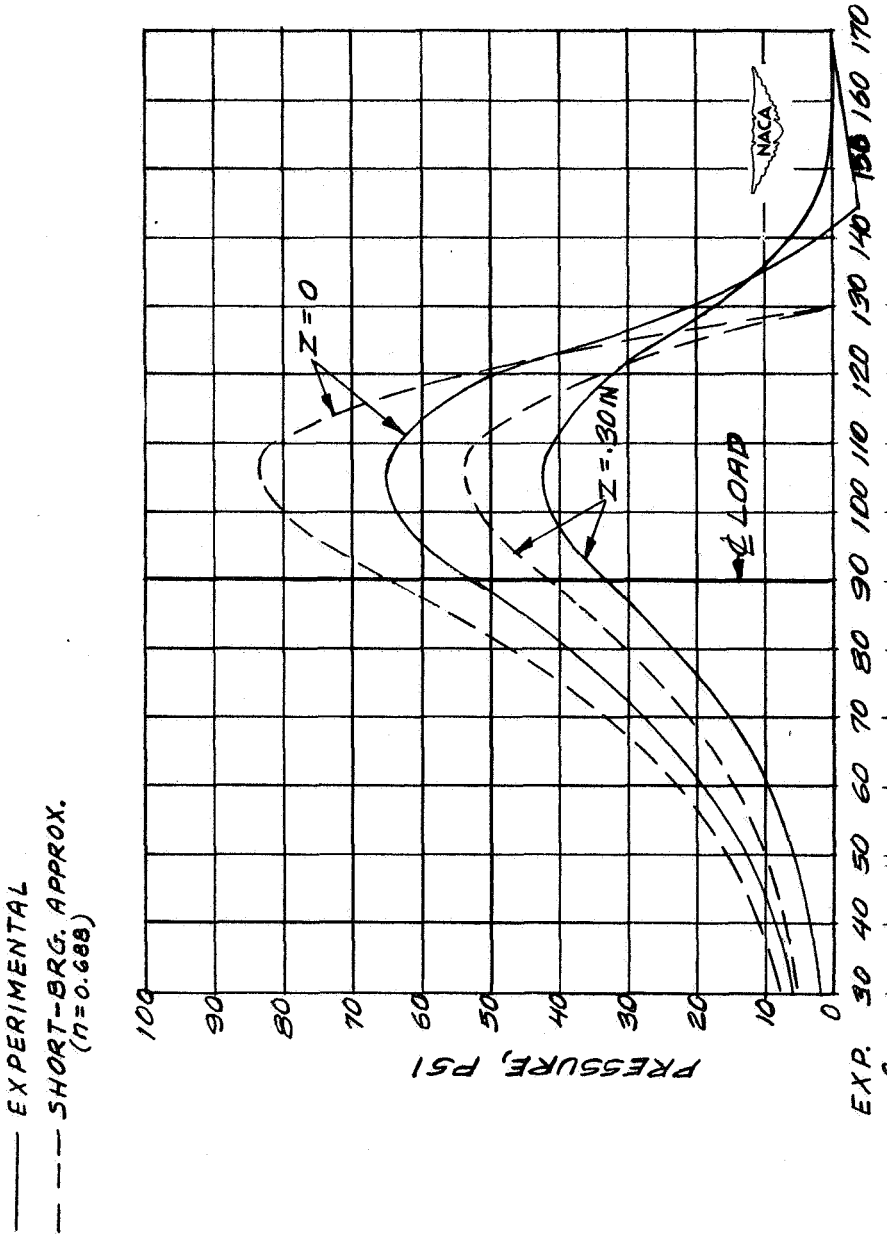

Figure 25.- Comparison of analytical pressure distribution with experimental pressure distribution from test no. 4 by McKee and McKee (reference 12). Load, 20 pounds; speed, 244 rpm; viscosity, 34.4 centipoises; bearing length, 1.0 inch; bearing diameter, 0.8703 inch; radial clearance, 0.0025 inch.

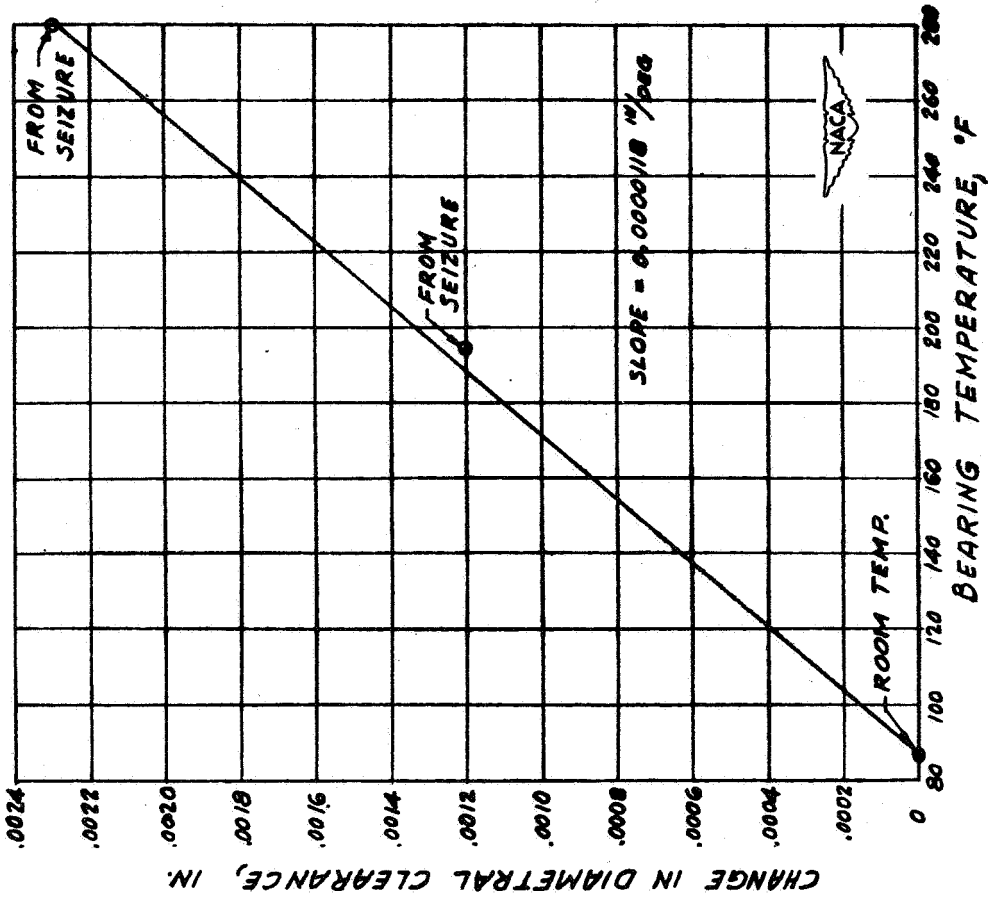

Figure 26.- Change in diametral clearance as function of bearing temperature caused by differential thermal expansion of journal and bearing. Data for journal bearing of model 2 (reference 14).

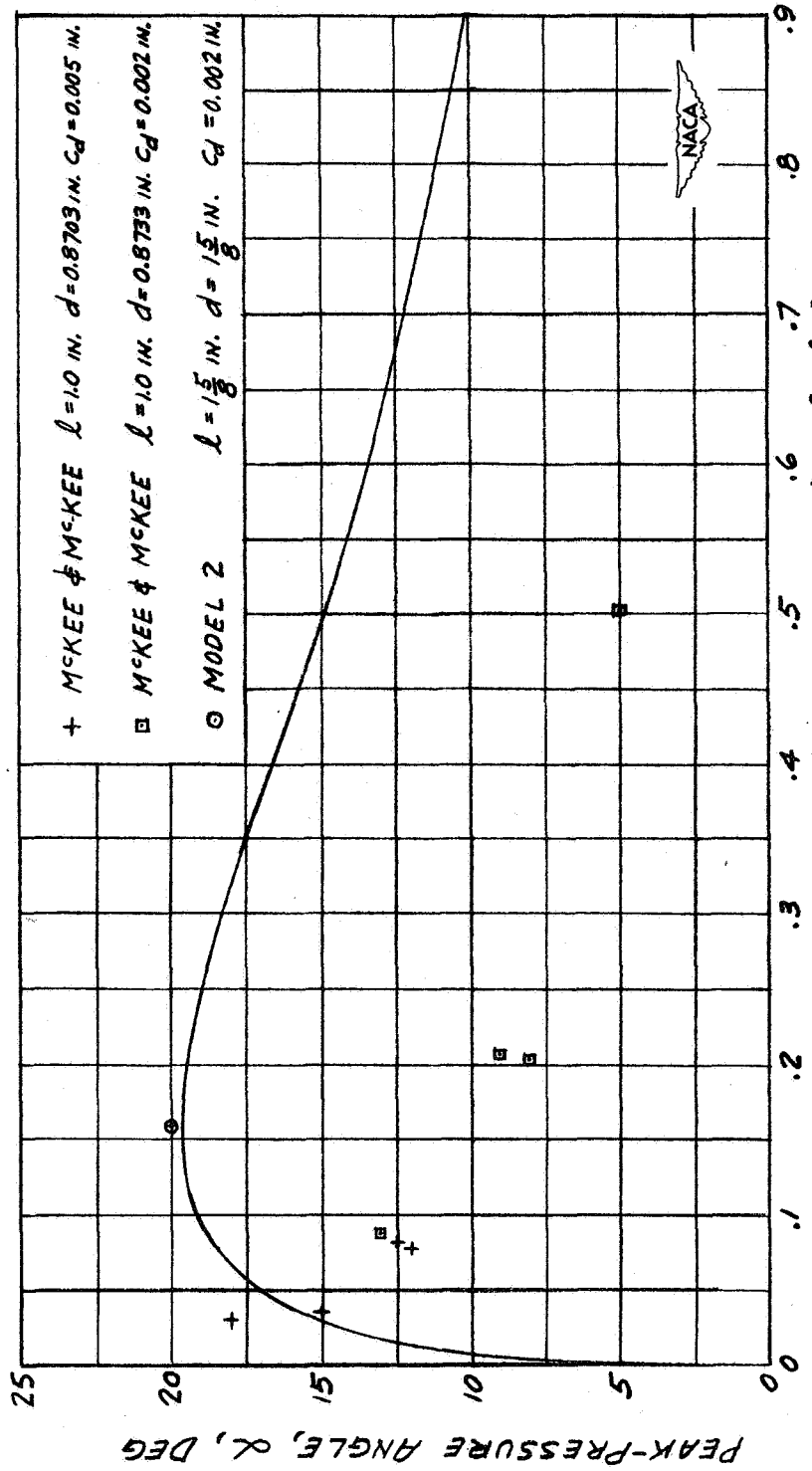

Figure 27.- Plot of peak-pressure angle against capacity number for comparison of experimental data with analytical curve for short bearings. Data by McKee and McKee taken from reference 12 and for model 2, from reference 14.

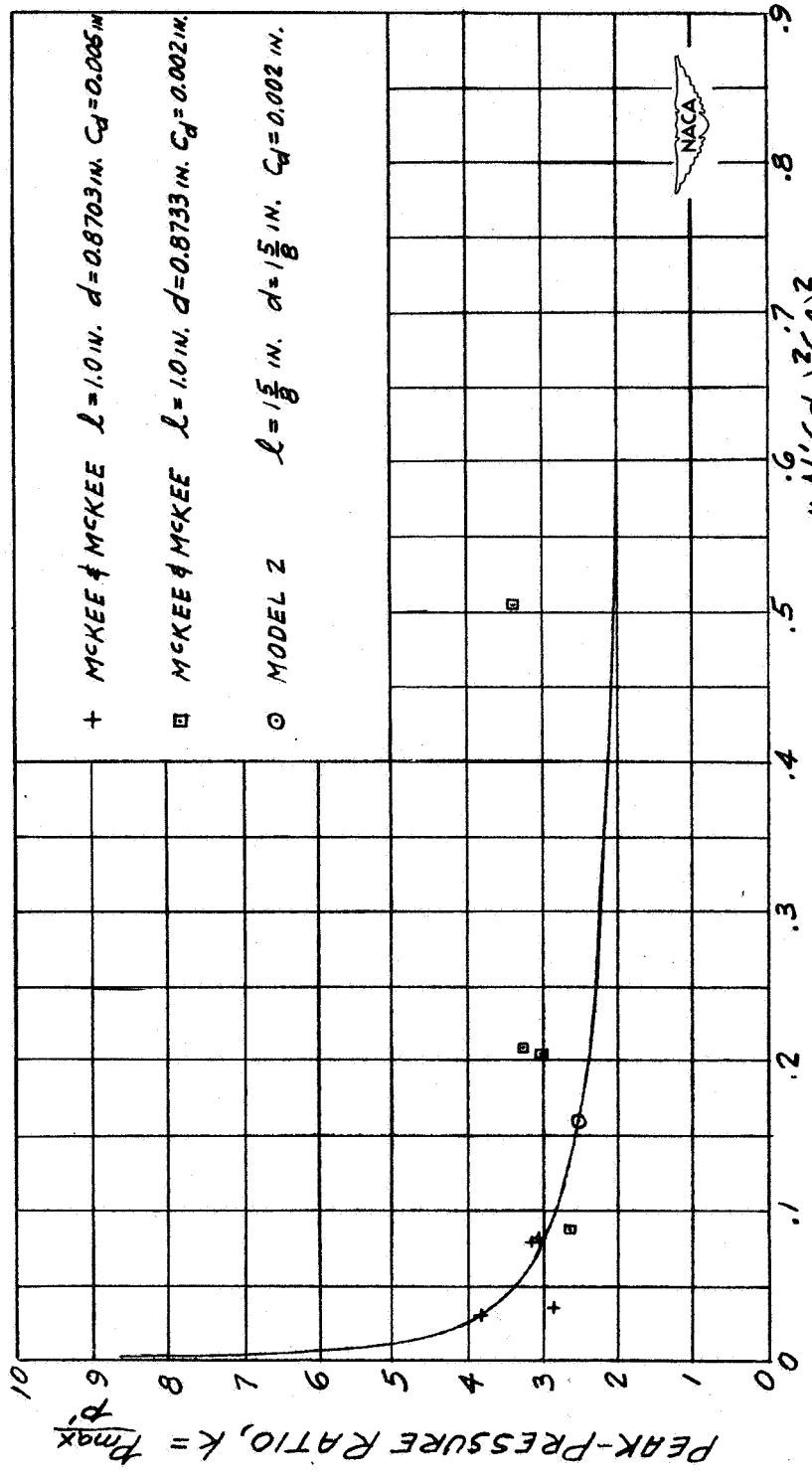

Figure 28.- Plot of peak-pressure ratio against capacity number for comparison of experimental data with analytical curve for short bearings. Data by McKee and McKee taken from reference 12 and for model 2, from reference 14.

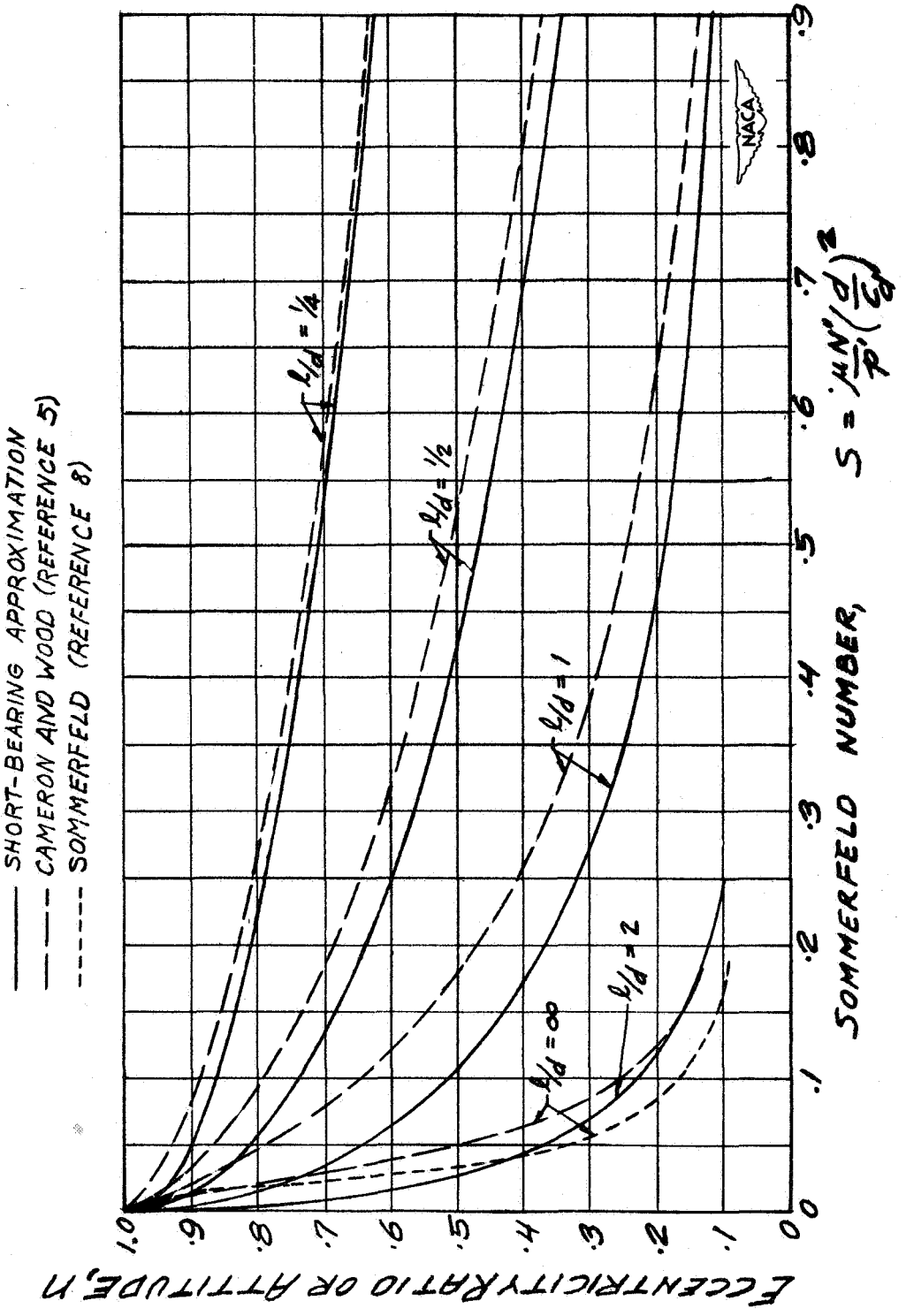

Figure 29.- Eccentricity ratio plotted against Sommerfeld number for comparison of theoretical curves.

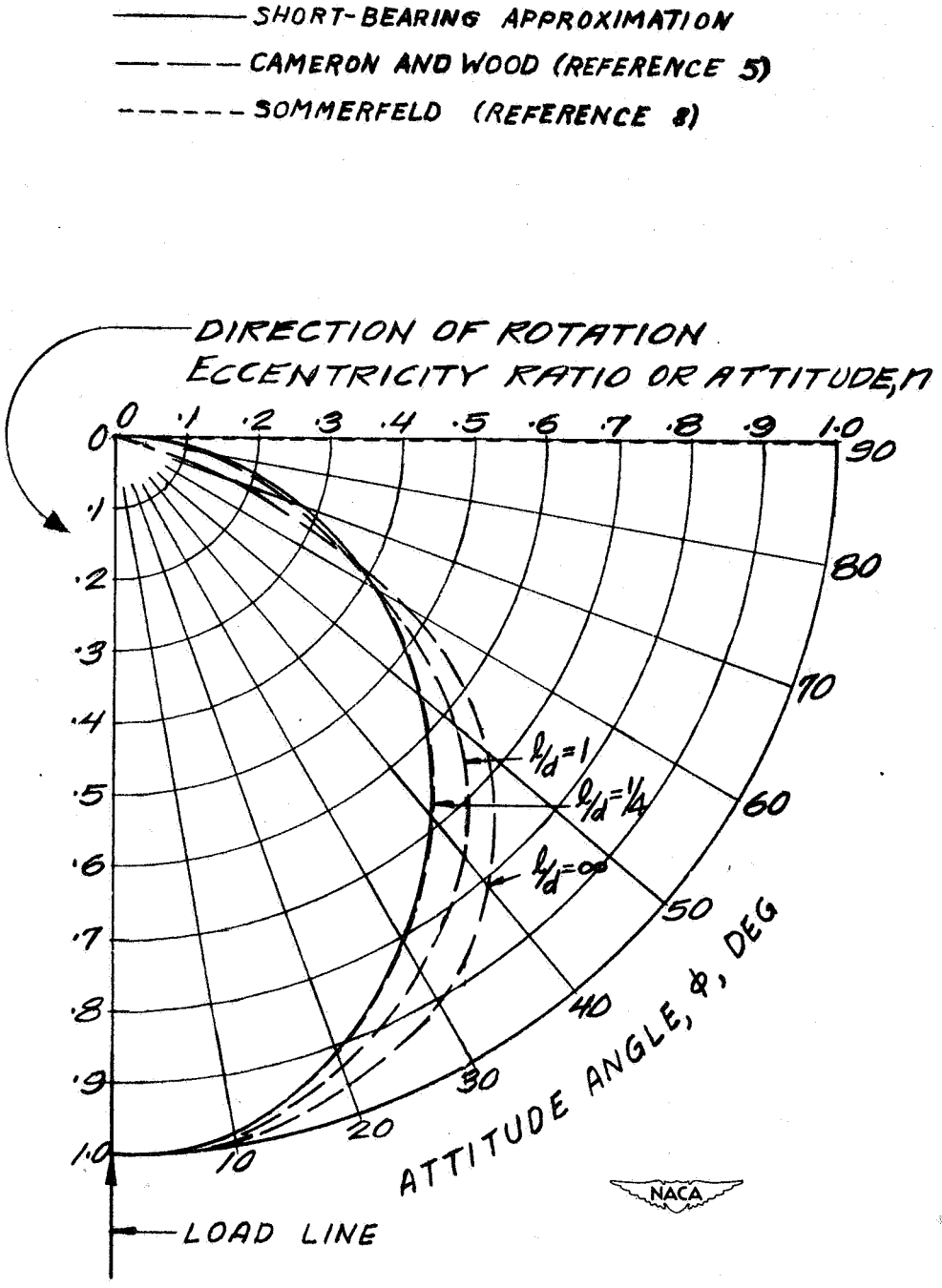

Figure 30.- Eccentricity ratio plotted against attitude angle for comparison of theoretical curves.

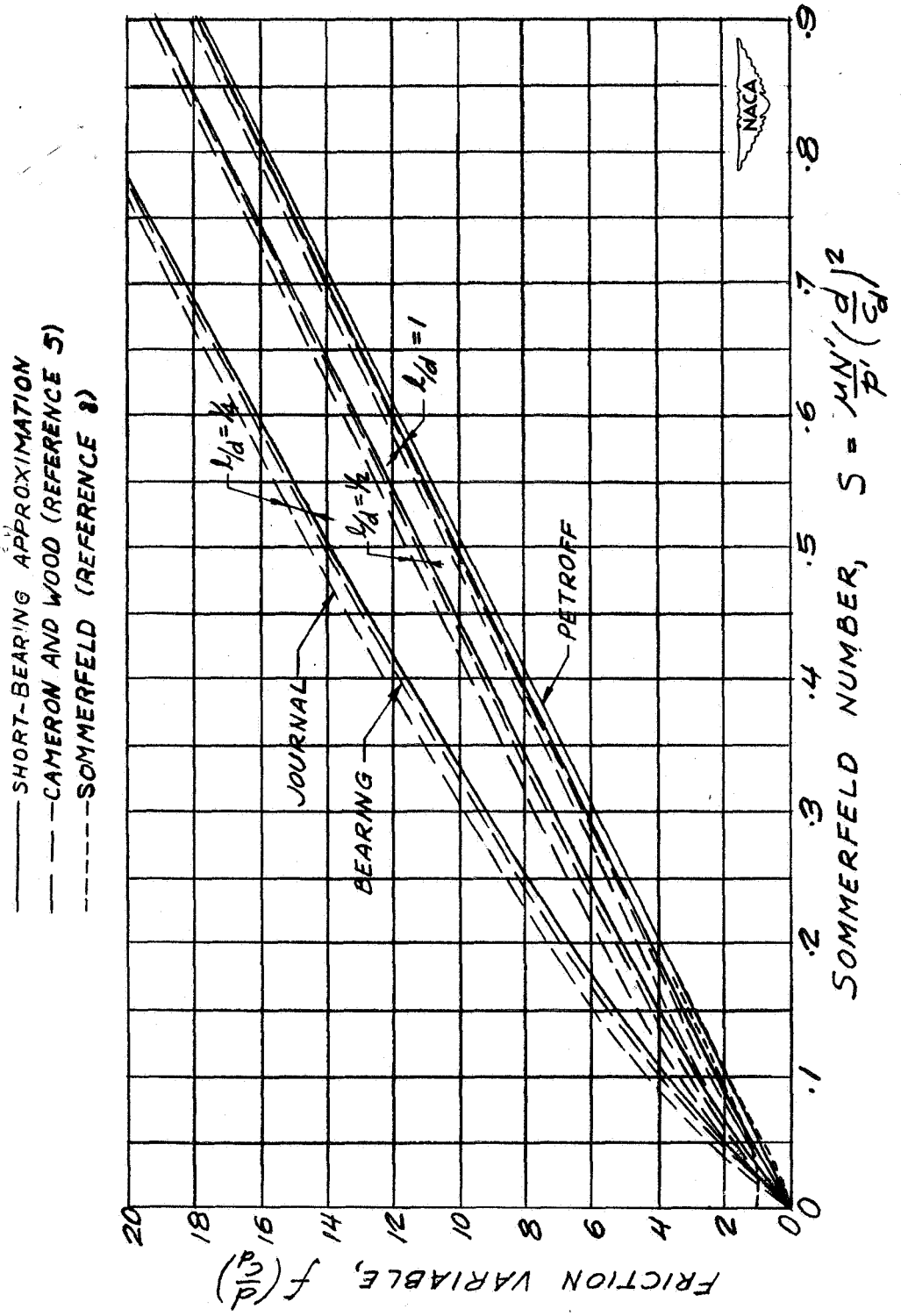

Figure 31.- Friction variable plotted against Sommerfeld number for comparison of theoretical curves.